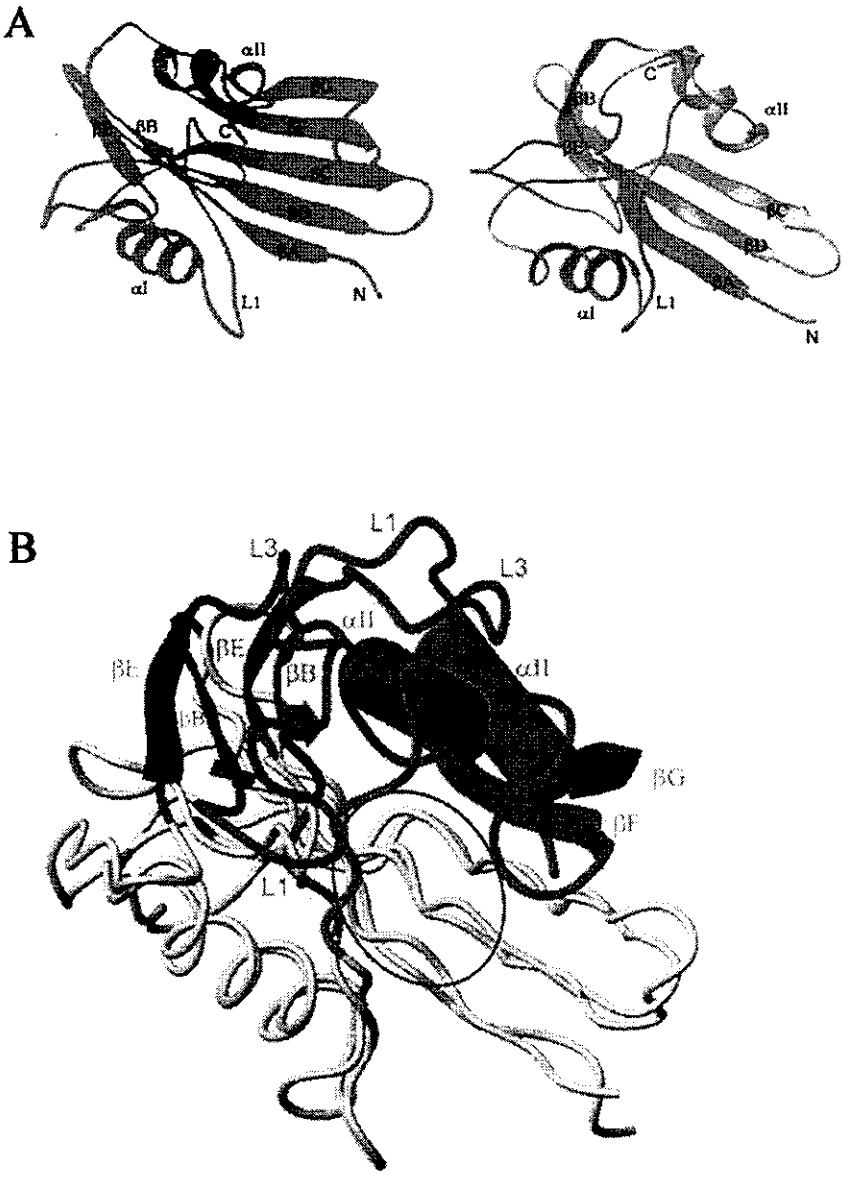

FIG. 4. **Comparison of the structures of MTH1 and *E. coli* MutT.** *A*, ribbon representations of MTH1 (*left*) and MutT (*right*; PDB code 1MUT), colored in *cyan* and *green*, respectively. The molecular orientation of MTH1 is nearly the same as in Fig. 1, *A* and *B*. *B*, superposition of MTH1 and MutT. MTH1 and MutT are shown in *magenta* and *green*, respectively. The nucleotide-binding pocket of MutT is *circled* in *red*.

Determination of the Site of Nucleophilic Attack on the Triphosphate—MTH1-mediated cleavage of the substrate Pα–Pβ bond is initiated by nucleophilic attack by water on either the α-phosphate (Pα) (Fig. 7*A*, *scheme 1*) or the β-phosphate (Pβ) (*scheme 2*). In order to determine which phosphate is attacked by water, we employed the isotope-labeling method of Mildvan and co-workers (29, 31). In this experiment, hydrolysis reactions are carried out in the presence of H_2O enriched with ^{18}O. Given that an oxygen atom of the water-attacked phosphate is substituted by that of water, the phosphate group of either 8-oxo-dGMP or pyrophosphate will be labeled with ^{18}O, depending on whether Pα or Pβ is attacked by water. On the one hand, if nucleophilic substitution by water occurs at the Pα site, ^{18}O-labeled 8-oxo-dGMP will be generated. On the other hand, if nucleophilic substitution occurs at the Pβ site, ^{18}O-labeled pyrophosphate will be generated. The compound that is labeled can be easily determined from ^{31}P NMR spectra of the reaction mixture, because the phosphorus attached to ^{18}O will exhibit a chemical shift difference because of the isotope effect.

The ^{31}P spectra of reaction mixtures are shown in Fig. 7, *A–C*. In the absence of ^{18}O-enriched water, the proton-decoupled ^{31}P NMR of the mixture showed two signals at about 2.52 and −7.75 ppm, which were attributable to the phosphates of 8-oxo-dGMP and pyrophosphate, respectively (Fig. 7*B*). When the reaction was carried out in the presence of 48% $H_2{}^{18}O$, a new peak appeared 0.012 ppm up field from the signal at −7.75 ppm (Fig. 7*C*). This chemical shift difference of 0.012 ppm is very similar to previously observed isotope effects caused by the incorporation of ^{18}O into phosphate (31). Therefore, it can be concluded that the new signal is attributable to ^{18}O-labeled pyrophosphate, and thus that Pβ of the substrate is attacked by water during the cleavage reaction. This cleavage site was further confirmed by carrying out the reaction in the presence of 24% $H_2{}^{18}O$, where the intensity of the new signal decreased to nearly half of the value observed for the reaction in the presence of 48% $H_2{}^{18}O$ (Fig. 7*D*).

DISCUSSION

The Nudix Motif—Saturation mutagenesis study has shown that 14 of the 23 conserved residues in the Nudix motif (residues 39, 41, 43, 45, 48, 51, 52, 53, 55, 56, and 57) are essential for catalysis by MTH1 (56). Of these, Glu^{52}, Glu^{55}, and Glu^{56} form an acidic cluster on the Nudix helix in our structure determination of MTH1 (Fig. 6*A*). These residues probably function to coordinate the catalytic metal ion, because the same residues in two other Nudix enzymes, MutT (55) and ADP-

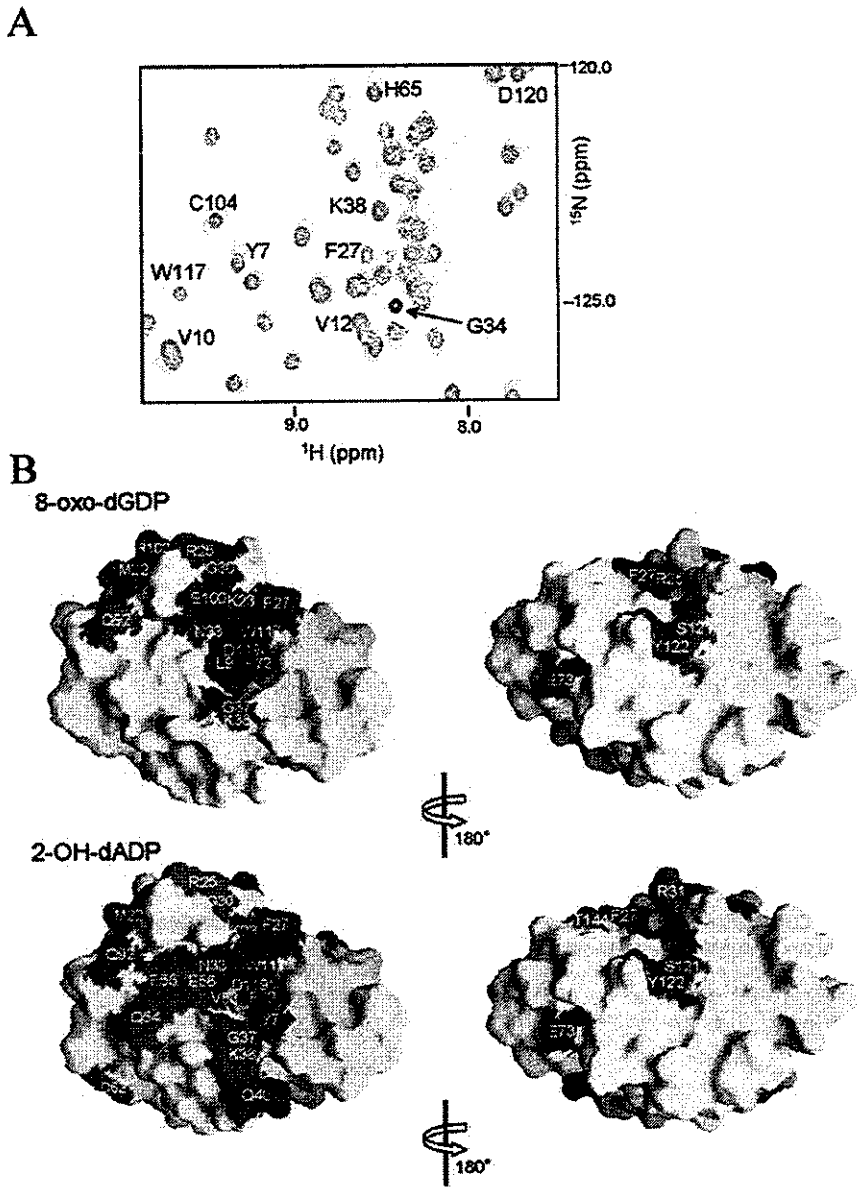

FIG. 5. **Chemical shift perturbation experiments.** *A*, selected region of the ^{15}N-^{1}H HSQC spectra of MTH1, recorded in the absence (*blue*) and presence (*red*) of an equimolar amount of 8-oxo-dGDP. *B*, representations of the protein surface with color coding to show the effects of titration with 8-oxo-dGDP (*upper*) and 2-OH-dADP (*lower*). The orientations of the molecular surfaces on the *right* are the same as in Fig. 1, *A* and *B*. Residues that showed a weighted average shift difference, $\delta_{ave}/\delta_{max}$ value, larger than 0.4 upon addition of the nucleotides are shown in *magenta*. Residues whose signal intensities were strongly reduced upon addition of nucleotide ($(I_{ref} - I_{per})/I_{ref} > 0.4$ of the original values) are shown in *red*. Residues whose values of both weighted average shift difference and intensity reduction were larger than the threshold values are also shown in *red*.

ribose pyrophosphatase (ADPRase) (57, 58), have been shown to bind the catalytic divalent metal. Two more acidic residues, Glu^{100} and Asp^{99}, are located within the vicinity of these acidic residues (Fig. 3). Our preliminary mutational analyses have shown that replacing Glu^{100} with alanine causes a total loss of catalytic activity, whereas a mutant in which Asp^{99} is replaced with alanine retains 91 and 79% of the wild-type activity for the hydrolysis of 2-OH-dATP and 8-oxo-dGTP, respectively,[2] indicating that Glu^{100}, but not Asp^{99}, is critical for catalytic activity. Structural determinations have shown that Glu^{100} of *E. coli* ADPRase, Glu^{98} of MutT (55), and Glu^{142} of *Mycobacterium tuberculosis* ADPRase (58) are metal-coordinating residues located outside the Nudix motif. In relation to the metal-coordinating Nudix residues, the structural position of these residues is similar to that of Glu^{100} of MTH1. These observations suggest that Glu^{100} of MTH1 functions as a metal-coordinating residue.

The moderately conserved hydrophobic residues in the Nudix motif correspond to residues Ala^{49}, Leu^{53}, and Leu^{59} of MTH1, which are located on the inner side of the helix, opposite the acidic metal-coordinating residues. These residues are important for packing the Nudix helix against the β-sheet and contribute to a hydrophobic core involving Thr^{8}, Val^{10}, and Val^{12} from strand βA, Phe^{86} from strand βD, and Phe^{35} from loop L1 (Fig. 3). Saturated mutagenesis study has shown that

[2] For preliminary measurement of the 8-oxo-dGTPase and 2-OH-dATPase activities of mutant enzymes, the MTH1 mutants E100A, D99A, N33A, and N33E were prepared by recombinant PCR. Their hydrolase activities were measured essentially as described previously (53) and are reported as a percentage of the wild-type activity. Each activity was measured in units/μg MTH1 at 120 min (1 unit of enzyme activity is equivalent to the production of 1 pmol of 8-oxo-dGMP or 2-OH-dAMP per min).

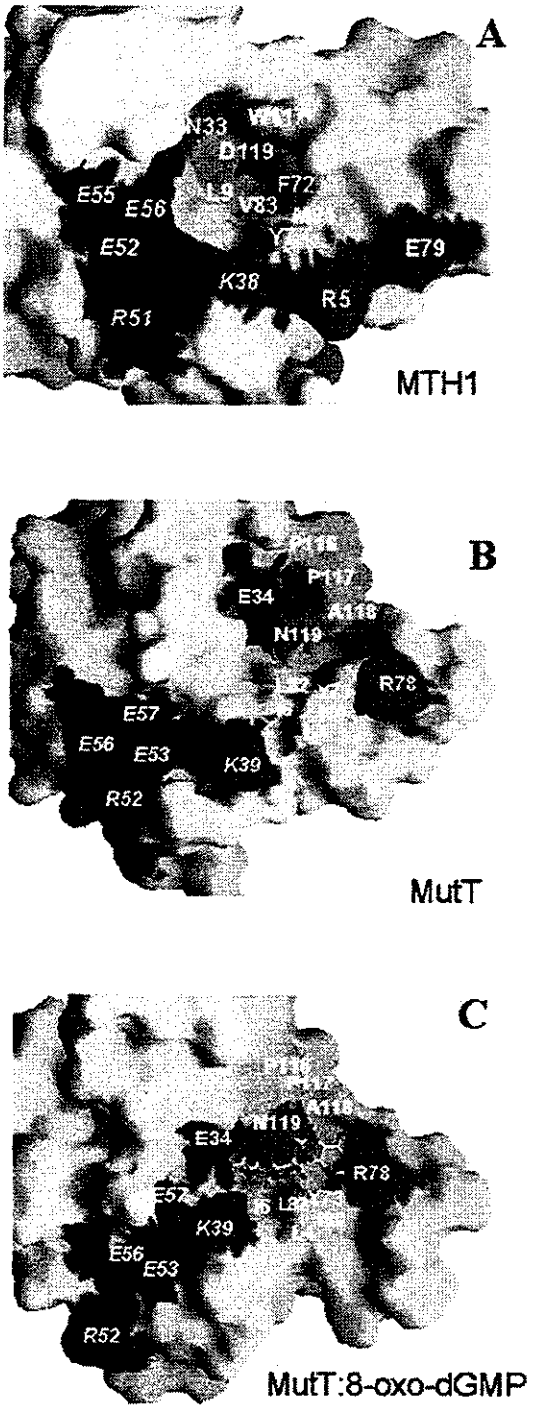

FIG. 6. **Comparison of the nucleotide-binding pockets of MTH1 and *E. coli* MutT.** Shown are the molecular surface representations of the nucleotide-binding pocket of MTH1 (*A*) and *E. coli* MutT (*B* and *C*). Hydrophobic residues are colored in *yellow*, acidic residues in *red*, basic residues in *blue*, and a polar residue in *green*. The molecular orientation of MTH1 is almost the same as in Fig. 1*A*. Structures of both the MutT (*B*; PDB code 1MUT) and MutT-8-oxo-dGMP (*C*; PDB code 1PUQ) complexes are shown. The nucleotides are shown in *ball-and-stick* representation. Residues in the Nudix motif are indicated in *italics*.

Leu[53] cannot be replaced with another residue without losing hydrolase activity (56). By contrast, Ala[49] can be replaced with serine; however, the expression level of A49S mutants is significantly low (56), indicating that the mutant protein is less stable than the wild-type protein. These observations suggest that both Ala[49] and Leu[53] may be important for maintaining the fold of the protein. The packing of the Nudix helix against the β-sheet is further stabilized by hydrophobic contact between Leu[59] located at the C terminus of the Nudix motif and both Leu[19] from strand βB and Val[12] from the C-terminal stretch of strand βA (Fig. 3).

In addition to the helix, the conformation of the preceding loop in the Nudix motif, located at residues 37–43, seems to be important for catalytic activity. This loop contains a β-turn at Gly[42], which is stabilized by a hydrogen bond formed between the side-chain carboxyl group of Glu[43] and the main-chain amide group of Gln[40]. Both Gly[42] and Glu[43] are highly conserved among Nudix enzymes. Glu[43] has been shown to be essential in mutagenesis studies (57, 60). This residue is unlikely to bind the metal ion, as shown by previous structural studies of MutT-AMPCPP (55), *E. coli* ADPRase (57), and *M. tuberculosis* ADPRase (58); therefore, the hydrogen bond mediated by this residue is probably important for catalytic activity. The importance of Gly[42] has also been confirmed by mutagenesis. Replacement with either proline or threonine causes a reduction in the 8-oxo-dGTP-specific activity (to 32% of the wild-type activity) (56). The same mutagenesis study also highlighted the importance of other loop-forming residues, Val[39] and Ile[45], which cannot be replaced by another residue without loss of enzyme activity (56). These two residues make hydrophobic contact with each other, defining the β-hairpin conformation of the loop together with the β-turn-forming residues (Fig. 3).

The N-terminal residues of the hairpin loop in the Nudix motif, residues 37–40, create part of the rim of the hydrophobic pocket. Of these, Gly[37] is conserved across all Nudix enzymes and is essential for catalytic activity as it cannot be replaced without loss of activity (57). The Hα1 proton of this residue is in close proximity to the side chain of the metal-coordinating residue Glu[52] (Fig. 3). Therefore, replacement of Gly[37] with another amino acid probably alters the local structure of the catalytic site residues, thereby leading to a loss of enzyme activity.

Important Residues for Recognition of the Oxidized Bases—Previous mutational analyses suggest that two of the pocket-forming residues of MTH1, Trp[117] and Asp[119], contribute to substrate recognition (53). Replacement of Trp[117] with alanine significantly increases the K_m for both 8-oxo-dGTP and 2-OH-dATP (53). The involvement of this tryptophan residue has also been implied from fluorescence studies, which show that binding of 8-oxo-dGTP or 2-OH-dATP alters the intensity and wavelength of the fluorescence attributed to this tryptophan, indicating that it is located proximal to the binding site (59). The decrease in the fluorescence intensity of Trp[117] induced by 8-oxo-dGTP or 2-OH-dATP is larger than that induced by unoxidized nucleotides. In contrast to mutation of Trp[117], replacing Asp[119] with alanine exhibits different effects on the catalysis of 8-oxo-dGTP and 2-OH-dATP (53). The D119A mutant has about half of the wild-type activity for 8-oxo-dGTP but shows almost no activity for 2-OH-dATP, and the D119N mutant also has similar activities with the D119A, suggesting that the charged carboxyl group (COO^-) of the side chain but not C=O group is crucial for discriminating the 2-hydroxyadenine ring.

In addition to these key residues identified through previous mutagenesis, our structure determination suggested that Asn[33] is important for nucleotide binding because its side chain is exposed in the pocket (Fig. 6*A*). To examine whether Asn[33] is involved in nucleotide interactions, we replaced it with alanine or glutamate. The N33A mutation decreased catalytic activity toward 2-OH-dATP to 5% of the wild-type activity,[2] whereas the N33E mutant showed a relative activity of 53%, suggesting that the presence of the side-chain C=O group at this position

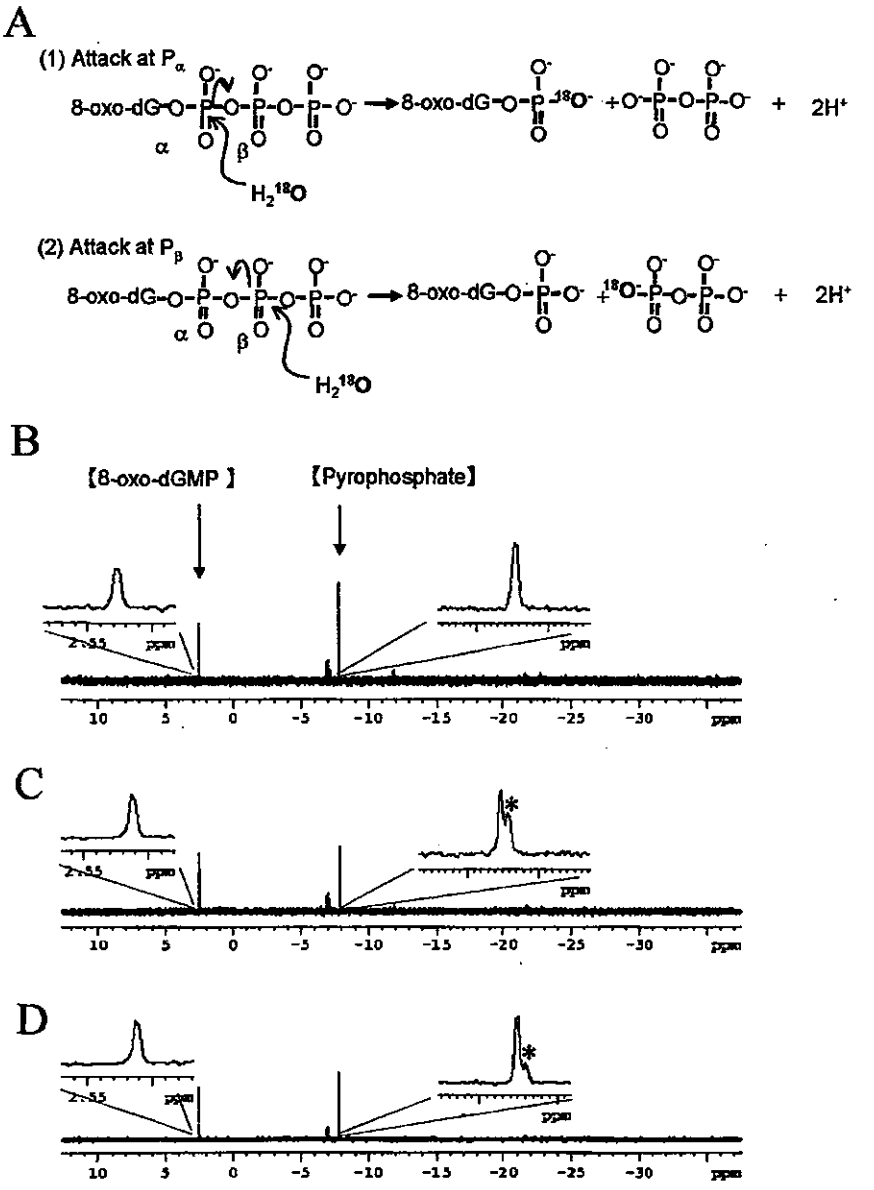

FIG. 7. **Mechanism of 8-oxo-dGTP hydrolysis by MTH1.** *A*, two possible pathways for the hydrolysis of 8-oxo-dGTP (1). The water molecule attacks at Pα, yielding ^{18}O-labeled 8-oxo-dGMP and nonlabeled pyrophosphate (2). The water molecule attacks at Pβ, yielding nonlabeled 8-oxo-dGMP and ^{18}O-labeled pyrophosphate. *B*, products of the 8-oxo-dGTP hydrolysis reaction carried out in H_2O. No isotope shift was observed for either 8-oxo-dGMP or pyrophosphate. *C*, products of the 8-oxo-dGTP hydrolysis reaction carried out in 52% H_2O, 48% $H_2{}^{18}O$. An isotope shift was observed only for pyrophosphate (*asterisk*). *D*, products of the 8-oxo-dGTP hydrolysis reaction carried out in 76% H_2O, 24% $H_2{}^{18}O$. An isotope shift was observed only for pyrophosphate (*asterisk*), and the peak height was half the value in *C*.

is also important for recognizing 2-OH-dATP. Intriguingly, the N33A mutant showed 14% of the wild-type 8-oxo-dGTP activity, whereas the N33E mutation totally abolished 8-oxo-dGTPase activity.[2] The detrimental effect of this mutation on 8-oxo-dGTPase activity may be explained by a significant steric clash between the carboxyl group of the glutamate and 8-oxo-dGTP and charge repulsion between the carboxyl group of the glutamate.

In summary, these structural and mutagenesis studies suggest that the side chains of Asp^{119} and Asn^{33} play an essential role in 2-OH-dATP recognition, whereas the indole ring of Trp^{117} may be important for interacting with the purine bases of substrate nucleotides.

Conclusion—A characteristic feature of MTH1 is its dual specificity for nucleotides that contain 2-OH-adenine bases and those that contain 8-oxo-guanine bases, whose oxidization sites are located at the opposite side of the purine rings to each other. Together with previous mutagenesis studies, our present study has enabled us to identify the 2-OH-dATP- and 8-oxo-dGTP-binding pocket of MTH1. On the basis of the structure determined, we performed additional mutagenesis studies that revealed that Asn^{33} also plays important role in 2-OH-dATP recognition.

To our knowledge, this *is* the first report of the tertiary structure of a enzyme that is known to recognize oxidized adenine. Although more than 130 proteins that contain a Nudix motif have been identified thus far (30), detailed substrate interactions have been well characterized for only a few of these enzymes. Our work has shown that MTH1 is similar to, but distinct from, *E. coli* MutT, with respect to the structure of the substrate-binding pocket. Our study may provide a structural basis for investigating substrates of the remaining orphan Nudix enzymes, as well as substrates of proteins that recognize oxidized nucleotides.

REFERENCES

1. Boiteux, S., Gajewski, E., Laval, J., and Dizdaroglu, M. (1992) *Biochemistry* **31**, 106–110
2. Gajewski, E., Rao, G., Nackerdien, Z., and Dizdaroglu, M. (1990) *Biochemistry* **29**, 7876–7882
3. Maki, H., and Sekiguchi, M. (1992) *Nature* **355**, 273–275
4. Cheng, K. C., Cahill, D. S., Kasai, H., Nishimura, S., and Loeb, L. A. (1992) *J. Biol. Chem.* **267**, 166–172
5. Kamiya, H., Murata-Kamiya, N., Koizume, S., Inoue, H., Nishimura, S., and Ohtsuka, E. (1995) *Carcinogenesis* **16**, 883–889
6. Tchou, J., Kasai, H., Shibutani, S., Chung, M. H., Laval, J., Grollman, A. P., and Nishimura, S. (1991) *Proc. Natl. Acad. Sci. U. S. A.* **88**, 4690–4694
7. Michaels, M. L., Cruz, C., Grollman, A. P., and Miller, J. H. (1992) *Proc. Natl. Acad. Sci. U. S. A.* **89**, 7022–7025
8. Michaels, M. L., and Miller, J. H. (1992) *J. Bacteriol.* **174**, 6321–6325

9. Tajiri, T., Maki, H., and Sekiguchi, M. (1995) *Mutat. Res.* **336,** 257–267
10. Yanofsky, C., Cox, E. C., and Horn, V. (1966) *Proc. Natl. Acad. Sci. U. S. A.* **55,** 274–281
11. Akiyama, M., Maki, H., Sekiguchi, M., and Horiuchi, T. (1989) *Proc. Natl. Acad. Sci. U. S. A.* **86,** 3949–3952
12. Bessho, T., Tano, K., Kasai, H., Ohtsuka, E., and Nishimura, S. (1993) *J. Biol. Chem.* **268,** 19416–19421
13. McGoldrick, J. P., Yeh, Y. C., Solomon, M., Essigmann, J. M., and Lu, A. L. (1995) *Mol. Cell. Biol.* **15,** 989–996
14. Oda, H., Nakabeppu, Y., Furuichi, M., and Sekiguchi, M. (1997) *J. Biol. Chem.* **272,** 17843–17850
15. Kang, D., Nishida, J., Iyama, A., Nakabeppu, Y., Furuichi, M., Fujiwara, T., Sekiguchi, M., and Takeshige, K. (1995) *J. Biol. Chem.* **270,** 14659–14665
16. Tsuzuki, T., Egashira, A., Igarashi, H., Iwakuma, T., Nakatsuru, Y., Tominaga, Y., Kawate, H., Nakao, K., Nakamura, K., Ide, F., Kura, S., Nakabeppu, Y., Katsuki, M., Ishikawa, T., and Sekiguchi, M. (2001) *Proc. Natl. Acad. Sci. U. S. A.* **98,** 11456–11461
17. Kennedy, C. H., Cueto, R., Belinsky, S. A., Lechner, J. F., and Pryor, W. A. (1998) *FEBS Lett.* **429,** 17–20
18. Iida, T., Furuta, A., Kawashima, M., Nishida, J., Nakabeppu, Y., and Iwaki, T. (2001) *Neuro-oncol.* **3,** 73–81
19. Shimura-Miura, H., Hattori, N., Kang, D., Miyako, K., Nakabeppu, Y., and Mizuno, Y. (1999) *Ann. Neurol.* **46,** 920–924
20. Furuta, A., Iida, T., Nakabeppu, Y., and Iwaki, T. (2001) *Neuroreport* **12,** 2895–2899
21. Fujikawa, K., Kamiya, H., Yakushiji, H., Fujii, Y., Nakabeppu, Y., and Kasai, H. (1999) *J. Biol. Chem.* **274,** 18201–18205
22. Fujikawa, K., Kamiya, H., Yakushiji, H., Nakabeppu, Y., and Kasai, H. (2001) *Nucleic Acids Res.* **29,** 449–454
23. Inoue, M., Kamiya, H., Fujikawa, K., Ootsuyama, Y., Murata-Kamiya, N., Osaki, T., Yasumoto, K., and Kasai, H. (1998) *J. Biol. Chem.* **273,** 11069–11074
24. Yoshimura, D., Sakumi, K., Ohno, M., Sakai, Y., Furuichi, M., Iwai, S., and Nakabeppu, Y. (2003) *J. Biol. Chem.* **278,** 37965–37973
25. Jaruga, P., and Dizdaroglu, M. (1996) *Nucleic Acids Res.* **24,** 1389–1394
26. Ishibashi, T., Hayakawa, H., and Sekiguchi, M. (2003) *EMBO Rep.* **4,** 479–483
27. Bessman, M. J., Frick, D. N., and Handley, S. F. (1996) *J. Biol. Chem.* **271,** 25059–25062
28. Dunn, C. A., O'Handley, S. F., Frick, D. N., and Bessman, M. J. (1999) *J. Biol. Chem.* **274,** 32318–32324
29. O'Handley, S. F., Frick, D. N., Bullions, L. C., Mildvan, A. S., and Bessman, M. J. (1996) *J. Biol. Chem.* **271,** 24649–24654
30. Sheikh, S., O'Handley, S. F., Dunn, C. A., and Bessman, M. J. (1998) *J. Biol. Chem.* **273,** 20924–20928
31. Weber, D. J., Bhatnagar, S. K., Bullions, L. C., Bessman, M. J., and Mildvan, A. S. (1992) *J. Biol. Chem.* **267,** 16939–16942
32. Yakushiji, H., Maraboeuf, F., Takahashi, M., Deng, Z. S., Kawabata, S., Nakabeppu, Y., and Sekiguchi, M. (1997) *Mutat. Res.* **384,** 181–194
33. Hall, T. A. (1999) *Nucleic Acids Symp. Ser.* **41,** 95–98
34. Muhandiram, D. R., and Kay, L. E. (1994) *J. Magn. Reson.* **103,** 203–216
35. Kay, L. E., Xu, G. Y., and Yamazaki, T. (1994) *J. Magn. Reson.* **129,** 129–133
36. Delaglio, F., Grzesiek, S., Vuister, G. W., Zhu, G., Pfeifer, J., and Bax, A. (1995) *J. Biomol. NMR* **6,** 277–279
37. Goddard, T. D., and Kneller, D. G. (1999) *SPARKY3*, University of California, San Francisco
38. Cavanagh, J., Fairbrother, W. J., Palmer, A. G., III, and Skelton, N. J. (1996) *Protein NMR Spectroscopy*, Academic Press, San Diego
39. Neri, D., Szyperski, T., Otting, G., Senn, H., and Wuthrich, K. (1989) *Biochemistry* **28,** 7510–7516
40. Cordier, F., and Grzesiek, S. (1999) *J. Am. Chem. Soc.* **121,** 1601–1602
41. Cornilescu, G., Hu, J. S., and Bax, A. (1999) *J. Am. Chem. Soc.* **121,** 2949–2950
42. Pellecchia, M., Iwai, H., Szyperski, T., and Wuthrich, K. (1997) *J. Magn. Reson.* **124,** 274–278
43. Nilges, M. (1995) *J. Mol. Biol.* **245,** 645–660
44. Cornilescu, G., Delaglio, F., and Bax, A. (1999) *J. Biomol. NMR* **13,** 289–302
45. Guntert, P., Mumenthaler, C., and Wuthrich, K. (1997) *J. Mol. Biol.* **273,** 283–298
46. Brunger, A. T., Adams, P. D., Clore, G. M., DeLano, W. L., Gros, P., Grosse-Kunstleve, R. W., Jiang, J. S., Kuszewski, J., Nilges, M., Pannu, N. S., Read, R. J., Rice, L. M., Simonson, T., and Warren, G. L. (1998) *Acta Crystallogr. Sect. D Biol. Crystallogr.* **54,** 905–921
47. Laskowski, R. A., Rullmannn, J. A., MacArthur, M. W., Kaptein, R., and Thornton, J. M. (1996) *J. Biomol. NMR* **8,** 477–486
48. Koradi, R., Billete, M., and Wuthrich, K. (1996) *J. Mol. Graphics* **14,** 51–55
49. Carson, M. J. (1991) *J. Appl. Crystallogr.* **24,** 379–384
50. Nicholls, A., Sharp, K. A., and Honig, B. (1991) *Protiens Struct. Funct. Genet.* **11,** 281–296
51. Garrett, D. S., Seok, Y. J., Peterkofsky, A., Clore, G. M., and Gronenborn, A. M. (1997) *Biochemistry* **36,** 4393–4398
52. Foster, M. P., Wuttke, D. S., Clemens, K. R., Jahnke, W., Radhakrishnan, I., Tennant, L., Reymond, M., Chung, J., and Wright, P. E. (1988) *J. Biomol. NMR* **12,** 51–71
53. Sakai, Y., Furuichi, M., Takahashi, M., Mishima, M., and Iwai, S., Shirakawa, M., and Nakabeppu, Y. (2002) *J. Biol. Chem.* **277,** 8579–8587
54. Massiah, M. A., Saraswat, V., Azurmendi, H. F., and Mildvan, A. S. (2003) *Biochemistry* **42,** 10140–10154
55. Lin, J., Abeygunawardana, C., Frick, D. N., Bessman, M. J., and Mildvan, A. S. (1997) *Biochemistry* **36,** 1199–1211
56. Fujii, Y., Shimokawa, H., Sekiguchi, M., and Nakabeppu, Y. (1999) *J. Biol. Chem.* **274,** 38251–38259
57. Gabelli, S. B., Bianchet, M. A., Bessman, M. J., and Amzel, L. M. (2001) *Nat. Struct. Biol.* **5,** 467–472
58. Kang, L. W., Gabelli, S. B., Cunningham, J. E., O'Handley, S. F., and Amzel, L. M. (2003) *Structure* **11,** 1015–1023
59. Takahashi, M., Maraboeuf, F., Sakai, Y., Yakushiji, H., Mishima, M., Shirakawa, M., Iwai, S., Hayakawa, H., Sekiguchi, M., and Nakabeppu, Y. (2002) *J. Mol. Biol.* **319,** 129–139
60. Cai, J. P., Kakuma, T., Tsuzuki, T., and Sekiguchi, M. (1995) *Carcinogenesis* **16,** 2343–2350

MOLECULAR AND CELLULAR BIOLOGY, Jan. 2004, p. 465–474 Vol. 24, No. 1
0270-7306/04/$08.00+0 DOI: 10.1128/MCB.24.1.465–474.2004

The Oxidized Deoxynucleoside Triphosphate Pool Is a Significant Contributor to Genetic Instability in Mismatch Repair-Deficient Cells

Maria Teresa Russo,[1]† Monica Francesca Blasi,[1]† Federica Chiera,[1] Paola Fortini,[1] Paolo Degan,[2] Peter Macpherson,[3] Masato Furuichi,[4] Yusaku Nakabeppu,[4] Peter Karran,[3] Gabriele Aquilina,[1] and Margherita Bignami[1]*

Chemical Carcinogenesis Unit, Istituto Superiore di Sanità, Rome,[1] and Istituto Nazionale per la Ricerca sul Cancro, Genoa,[2] Italy; Clare Hall Laboratories, Cancer Research UK London Research Institute, South Mimms, United Kingdom[3]; and Department of Biochemistry, Kyushu University, Fukuoka, Japan[4]

Received 6 August 2003/Returned for modification 10 September 2003/Accepted 18 September 2003

Oxidation is a common form of DNA damage to which purines are particularly susceptible. We previously reported that oxidized dGTP is potentially an important source of DNA 8-oxodGMP in mammalian cells and that the incorporated lesions are removed by DNA mismatch repair (MMR). MMR deficiency is associated with a mutator phenotype and widespread microsatellite instability (MSI). Here, we identify oxidized deoxynucleoside triphosphates (dNTPs) as an important cofactor in this genetic instability. The high spontaneous *hprt* mutation rate of MMR-defective *msh2*$^{-/-}$ mouse embryonic fibroblasts was attenuated by expression of the hMTH1 protein, which degrades oxidized purine dNTPs. A high level of hMTH1 abolished their mutator phenotype and restored the *hprt* mutation rate to normal. Molecular analysis of *hprt* mutants showed that the presence of hMTH1 reduced the incidence of mutations in all classes, including frameshifts, and also implicated incorporated 2-oxodAMP in the mutator phenotype. In *hMSH6*-deficient DLD-1 human colorectal carcinoma cells, overexpression of hMTH1 markedly attenuated the spontaneous mutation rate and reduced MSI. It also reduced the incidence of −G and −A frameshifts in the *hMLH1*-defective DU145 human prostatic cancer cell line. Our findings indicate that incorporation of oxidized purines from the dNTP pool may contribute significantly to the extreme genetic instability of MMR-defective human tumors.

Mismatch repair (MMR) removes DNA mismatches that evade proofreading during replication. This versatile postreplicative repair system efficiently corrects single base mismatches and loops of one to three extrahelical nucleotides (insertion deletion loops [IDLs]) that arise during the replication of repetitive DNA tracts. IDLs are considered to be the result of spontaneous, slippage-dependent misalignment between primer and template DNA strands. Error correction is initiated by the binding by one of two mismatch recognition complexes that have overlapping specificities. This ensures efficient repair of all of the common replication errors. The hMutSα and hMutSβ mismatch recognition factors are heterodimers of hMSH2/hMSH6 and hMSH2/hMSH3, respectively. hMutSα preferentially initiates correction of base-base mismatches and small IDLs, whereas hMutSβ targets larger IDLs (for reviews, see references 26 and 31). Complete excision and replacement of the mismatched section of DNA also involves heterodimeric complexes between the hMLH1 and hPMS2 (or hMLH3) proteins, PCNA (43), RPA, DNA polymerase δ, and hEXO1 (44).

Because of its central role in replication error correction, cells in which MMR is incapacitated by inactivating mutations in *hMSH2*, *hMLH1*, *hPMS2*, or *hMSH6* have high spontaneous mutation rates. This mutator effect is observed as a dramatic increase in the frequency of base substitutions and frameshifts. Frameshifts derive from uncorrected IDLs and are generally located in repetitive DNA sequences. These are located within the coding sequences of genes, as well as in the numerous noncoding microsatellite regions distributed throughout the genome. Alterations in the length of multiple microsatellites are a characteristic feature of MMR-deficient cells, and this microsatellite instability (MSI) is diagnostic for MMR deficiency in both cell lines and tumors (1).

MSI is a defining feature of tumors arising in hereditary nonpolyposis colorectal cancer (HNPCC) families. HNPCC individuals have a germ line mutation in one of the MMR genes—most commonly *hMSH2* or *hMLH1*. The increased mutation rate that accompanies somatic inactivation of the second allele accelerates the development of colorectal and other typical cancers in these individuals. In addition to these familial cases, a significant proportion of sporadic cancers exhibit MSI. In these cases, epigenetic silencing of an MMR gene, most commonly *hMLH1*, inactivates MMR. Organs, tumors, and cell lines from MMR gene knockout mice recapitulate this genetic instability and display both increased mutation rates and MSI (for a review, see reference 11). By analogy to HNPCC, the cancer proneness of these mice is generally considered to reflect an increased rate of accumulation of inactivating mutations in key target genes that normally function to prevent unlimited cellular proliferation.

Although it has been generally assumed that the mutator phenotype of MMR-deficient cells reflects uncorrected spontaneous DNA polymerase errors (42), MMR is also known to process some altered or damaged DNA bases. For example, O^6-methylguanine, a lesion induced by treatment with methy-

* Corresponding author. Mailing address: Chemical Carcinogenesis Unit, Istituto Superiore di Sanità, Viale Regina Elena 299, 00161 Rome, Italy. Phone: 0039-06-49902355. Fax: 0039-06-49902580. E-mail: bignami@iss.it.

† M.T.R. and M.F.B. contributed equally to this work.

lating carcinogens, is known to miscode during DNA replication and DNA containing O^6-methylguanine base pairs is bound by hMutSα (10, 17, 30). As a result, MMR-defective cells are hypermutable by these agents (3) and this hypermutability by spontaneous DNA lesions is a potential contributor to the mutator phenotype.

Oxidation is a significant and constant source of spontaneous DNA damage. The oxidized purine 8-oxo-7,8-dihydroguanine (8-oxoG) is a particularly frequent DNA lesion that, during replication, can form base pairs with adenine (41) to promote the formation of G → T transversions (46, 12). The extent of the threat posed by DNA 8-oxoG is emphasized by the existence of a highly conserved three-tier system that protects against the mutagenic properties of 8-oxoG. Two complementary arms of the base excision repair (BER) pathway bring about the removal of 8-oxoG from DNA. In the first, the hOGG1 DNA glycosylase initiates excision of the oxidized purine from resting DNA in which 8-oxoG is paired with C. An additional BER pathway, initiated by the MYH DNA glycosylase, a homolog of the *Escherichia coli* MutY protein, removes adenine misincorporated opposite 8-oxoG during replication. This promotes the eventual removal of the oxidized purine from DNA via hOGG1-mediated processing of the 8-oxoG · C base pairs generated during repair. Purine dNTPs are also subject to oxidative damage, and the oxidized products are substrates for incorporation into DNA during replication. To avoid this, human cells sanitize the dNTP pool by hydrolyzing oxidized purine dNTPs. This degradation is carried out by hMTH1, a homolog of the *E. coli* MutT protein that hydrolyzes 8-oxodGTP (36).

There is mounting evidence that MMR also contributes to reducing the burden of oxidized DNA bases. Treatment of *E. coli* MMR mutants with H_2O_2 increases the instability of repetitive sequences in extrachromosomal plasmid DNA (25). In *Saccharomyces cerevisiae*, the mutator phenotype of *MSH2*- and *MSH6*-defective strains is significantly decreased by anaerobic growth, suggesting that a large fraction of spontaneous mutagenesis in MMR-deficient strains is caused by the persistence of oxidatively damaged bases (18). Yeast MMR processes 8-oxoG · A base pairs, and its ability to excise A incorporated opposite 8-oxoG may compensate for the apparent absence of a MutY homolog in this organism (37). The mammalian MMR system also participates in minimizing the levels of oxidative DNA damage. Thus, the steady-state level of DNA 8-oxoG is significantly elevated in MMR-deficient mouse (15) and human (14) cells. Consistent with this, hMutSα binds to some 8-oxoG-containing base pairs (35). The efficiency of excision of the oxidized purine by BER appears to be similar in MMR-proficient and -defective cells. We have provided evidence that MMR removes 8-oxodGMP incorporated during replication (14) and suggested that this new role for MMR represents a fourth level of protection against the dangers of oxidized DNA bases.

To determine the full impact of incorporated oxidized DNA precursors on spontaneous mutation in MMR-defective cells, we characterized spontaneous mutations in *msh2*$^{-/-}$ mouse embryo fibroblasts (MEFs) in which *hMTH1* cDNA is expressed. We also analyzed the influence of increased hMTH1 expression on MSI. The findings indicate that (i) the oxidized purine dNTP pool is a significant contributor to mutation in MMR-deficient cells, (ii) both 8-oxodGTP and 2-oxodATP are implicated in mutation, and (iii) incorporation of oxidized DNA precursors is a significant influence on MSI in repair-defective human tumor cells.

MATERIALS AND METHODS

Cell culture, DNA transfection, and analysis of hMTH1 activity in transfectants. All cells were grown routinely in Dulbecco's modified Eagle's medium supplemented with 10% fetal calf serum, penicillin (100 U/ml), and streptomycin (100 μg/ml) (Gibco-BRL). Cell lines were incubated at 37°C in a 5% CO_2 atmosphere (90% nominal humidity). Exponentially growing *msh2*$^{-/-}$ MEFs were transfected (Lipofectamine; GIBCO-BRL) with pcDEBdelta carrying hygromycin resistance together with the cDNA for hMTH1d, the major 18-kDa form of hMTH1 (29). Hygromycin (400 μg/ml; GIBCO-BRL)-resistant clones were isolated after 15 to 20 days. hMTH1 expression in transfectants was quantitated by measurement of dGTPase activity in cell extracts and monitored by Western blotting as previously described (14). For dGTPase determinations, extracts were prepared from 2×10^7 cells in 200 μl of 50 mM Tris-HCl (pH 7.5)–1 mM EDTA–10 mM dithiothreitol–0.2% Triton X-100. Reaction mixtures (20 μl) contained 20 mM Tris-HCl (pH 7.5), 8 mM $MgCl_2$, 5 mM dithiothreitol, 100 μM [α-^{32}P]dGTP (2 Ci/mmol; Amersham), and cell extract. Following 10 min of incubation at 37°C, reactions were terminated by chilling to 0°C and addition of EDTA to 10 mM. Aliquots (2.5 μl) were applied to thin-layer polyethyleneimine-cellulose plates, which were developed in 1 M LiCl. Dried plates were exposed to X-rays film, and dGTP and dGMP were quantitated by using the National Institutes of Health V1.59 software package. One unit of hMTH1 produces 1 pmol of dGMP per min in the standard assay. For Western blotting cell extracts were separated by sodium dodecyl sulfate–7.5% polyacrylamide gel electrophoresis, transferred to nitrocellulose membrane with a Trans-Blot cell apparatus (Bio-Rad), and probed overnight with anti-hMTH1 antibody, followed by the appropriate secondary antibody. Blots were developed by using the ECL detection reagents (Amersham).

8-OxoG determinations. 8-OxodG was measured by high-performance liquid chromatography with electrochemical detection (HPLC/EC) as previously described (7) following DNA extraction, RNase treatment, and enzymatic hydrolysis. DNA was extracted by a high-salt protein precipitation method. Briefly, cells were lysed with sodium dodecyl sulfate and digested with protease (Qiagen) at 37°C for 1 h. Proteins were precipitated by adding NaCl to 1.5 M, and DNA in the supernatant was collected by addition of 2 volumes of ethanol. The DNA pellet was resuspended in Tris-EDTA, incubated with RNases A and T1 at 37°C for 1 h, and precipitated again with ethanol. Enzymatic digestion was then performed at 37°C with nuclease P1 (Boehringer Mannheim) for 2 h and alkaline phosphatase (Boehringer Mannheim) for 1 h. Enzymes were precipitated by addition of $CHCl_3$, and the upper layer was stored for analysis of 8-oxodG at −80°C under N_2. The DNA hydrolysate was analyzed by HPLC/EC (Coulochem I; ESA Inc.) with a C_{18} 5-μm Uptishere column (250 by 46 mm; Interchim) equipped with a C_{18} guard column. The eluent was 50 mM ammonium acetate, pH 5.5, containing 9% methanol, at a flow rate of 0.7 ml/min. The potentials applied were 150 and 400 mV for E1 and E2, respectively. The retention time of 8-oxodG was ~23 min. Deoxyguanosine was measured in the same run of corresponding 8-oxodG with a UV detector (model SPD-2A; Shimadzu) at 256 nm; the retention time was ~17 min.

Mutation rate analysis at the *hprt* gene and DNA sequencing of mutants. Cells were plated at low density (100 cells/dish) and grown in complete medium to a density of 0.4×10^6 to 1×10^6 per dish before plating of the entire culture (50 to 60 independent cultures) into medium supplemented with 6-thioguanine (5 μg/ml; Sigma). The mutation rate was calculated as $\mu = M\,C^{-1}\ln 2$, where C is the number of cells at selection time and M is $-\ln(P_0)$, where P_0 is the proportion of cultures with no mutants. One 6-thioguanine-resistant mutant was isolated per culture to ensure mutation independence. Cytoplasmic RNA was extracted and used to synthesize *hprt* cDNA by SuperScript One-Step reverse transcription-PCR (Invitrogen) in a final volume of 50 μl containing 1 μg of RNA, 0.2 μM primers (45), RT/Platinum TaqMix (1 μl), and buffer provided with the enzyme. Cycles included 30 s at 55°C; 2 min at 94°C; 35 cycles of 15 s at 94°C, 30 s at 55°C, and 1 min at 72°C; and a final 10 min at 72°C. Reverse transcription-PCR products were cleaned with a QIAquick PCR purification kit (Qiagen), used in sequencing reactions (25 cycles of 10 s at 96°C, 5 s at 50°C, and 4 min at 60°C), and analyzed with an ABI Prism 310 automatic sequencer.

MSI. Genomic DNA was isolated from subclones of clonal isolates of DLD1, DLD1/clone 2A, DU145, and DU145/clone 1. Ninety-six-well plates were seeded at a density of <1 cell/well, and DNA was prepared from approximately 2×10^4

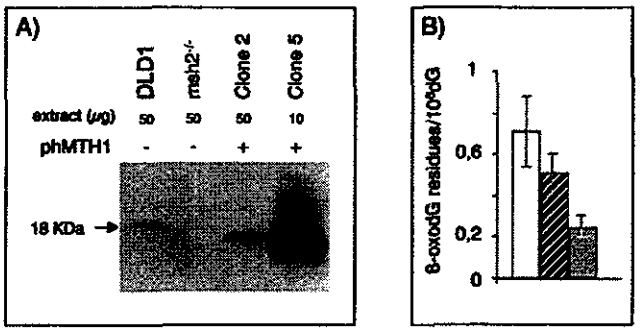

FIG. 1. Expression of hMTH1 in *msh2*-defective MEFs. (A) Western blot of *msh2*$^{-/-}$ MEFs. Clone 2 and 5 extracts were probed with antibody against hMTH1. The DLD1 human colorectal carcinoma cell line is shown for comparison. (B) Steady-state levels of DNA 8-oxoG in untransfected and *hMTH1*-transfected *msh2*$^{-/-}$ MEFs. DNA was extracted from exponentially growing cells, and 8-oxoG was determined by HPLC/EC as described in Materials and Methods. Values are the mean ± standard deviation of several independent determinations (n = 7 for *msh2*$^{-/-}$; n = 5 for clones 2 and 5). Data for untransfected *msh2*$^{-/-}$ MEFs (unfilled bar), clone 2 (hatched bar), and clone 5 (filled bar) are shown.

cells/well. DNA samples (10 ng) were used in PCRs with *BAT26*, *BAT25*, or *SMT15* primers (2 pmol/μl), dNTPs (200 mM) in a reaction buffer containing 0.5 U of *Taq* polymerase (Perkin-Elmer). Following the initial denaturation (95°C for 2 min), *BAT26* and *BAT25* were amplified by 35 cycles of 60 s at 95°C, 60s at 55°C, and 60 s at 72°C, followed by 10 min at 72°C. *SMT15* was amplified by using a four-stage protocol (49) as follows: four cycles of 30 s at 95°C, 30 s at 64°C, and 2 min at 70°C; four cycles of 30 s at 95°C, 30 s at 61°C, and 2 min at 70°C; four cycles of 30 s at 95°C, 30 s at 58°C, and 2 min at 70°C; and four cycles of 30 s at 95°C, 30 s at 55°C, and 2 min at 70°C. Amplification products (10 μl) were digested with 0.4 U of T4 DNA polymerase (Roche) for 30 min at 37°C, denatured in deionized formamide for 2 min at 95°C, and analyzed with an ABI Prism 310 automatic sequencer.

RESULTS

Biological consequences of hMTH1 overexpression. hMTH1 cDNA (29) was transfected into *msh2*-defective MEFs (14). hMTH1 expression in pooled transfectants and clonal isolates was measured by dGTPase assay and Western blotting. The low level of dGTPase activity in untransfected *msh2*$^{-/-}$ MEFs (0.4 U/mg of protein) was increased 10-fold in the pooled transfectants (pool 1) and also in a clonal isolate, clone 2, that contained 4.2 and 3.9 U/mg of protein, respectively. Screening of individual transfectants identified clone 5, in which dGTPase activity was increased around 50-fold, to 20.4 U/mg of protein. Western blotting of clone 2 and 5 extracts confirmed that the enhanced enzyme activity was correlated with an increased level of the hMTH1 protein (Fig. 1A). The apparent absence of the mouse MTH protein from untransfected *msh2*$^{-/-}$ extracts is most likely due to the low affinity of the human antibody for its mouse homolog since hMTH1 was detectable in Western blots of extracts of human DLD1 cells that contain comparable enzyme activity (0.6 U/mg of protein).

hMTH1 expressed in *msh2*$^{-/-}$ MEFs was active in excluding 8-oxodGMP from DNA. Direct measurements of DNA 8-oxodG in clones 2 and 5 confirmed that the steady-state level of the oxidized purine was significantly reduced from around 0.7 8-oxodG residues per 10^6 dGMP residues in nontransfected *msh2*$^{-/-}$ MEFs to 0.5 and 0.25 8-oxodG residues per 10^6 dGMP residues in clones 2 and 5, respectively (Fig. 1B).

hMTH1 expression reduced the mutator effect in *msh2*$^{-/-}$ MEFs. There was an inverse relationship between hMTH1 expression and the *hprt* mutation rate (Table 1). The rate in *msh2*$^{-/-}$ MEFs was 3.1×10^{-6} mutations/cell/generation (mean of the three independent determinations), a value 25-fold higher than rates in wild-type mouse cells (16). This value is compatible to the reported 10- to 20-fold increase in spontaneous mutation rates in *msh2*$^{-/-}$ mouse tissues (4). Modest hMTH1 overexpression (around 10 times the endogenous level) in the pooled transfectants and in clone 2 halved this to 1.4×10^{-6} mutations/cell/generation. The 50-fold-enhanced hMTH1 expression in clone 5 was associated with a 17-fold reduction to 0.18×10^{-6} mutations/cell/generation. This is close to the calculated values for wild-type mouse cells (16). (We were unable to calculate mutation rates in *msh2*$^{+/+}$ MEFs because of multiple copies of the *hprt* gene.) Transfection with the empty vector did not alter the *hprt* mutation frequency, and

TABLE 1. Mutation rates at the *hprt* gene in untransfected and *hMTH1*-expressing *msh2*$^{-/-}$ MEFs

Cells	No. of replica cultures	Final cell no. (10^5)	Fraction of culture without mutants (P_0)	Mutation rate (μ) ± SD (10^{-6})	Mean value of μ	Relative mutation rate decrease	hMTH1 activity (U/mg)
msh2$^{-/-}$ MEFs							
Expt 1	50	7.25	3/50	2.69 ± 0.40	3.06	1	0.4
Expt 2	50	5.32	15/50	1.57 ± 0.28			
Expt 3	44	4.33	2/44	4.29 ± 0.28			
hMTH1 pool 1	48	8.26	3/48	1.94 ± 0.39		1.6	4.2
hMTH1 clone 2							
Expt 1	10	10.69	1/10	1.49 ± 0.63	1.38	2.1	3.9
Expt 2	50	3.80	25/50	1.26 ± 0.25			
hMTH1 clone 5							
Expt 1	50	8.15	42/50	0.148 ± 0.052	0.18	16.9	20.4
Expt 2	50	12.30	41/50	0.112 ± 0.037			
Expt 3	54	12.00	33/54	0.284 ± 0.063			

TABLE 2. Class distribution of *hprt* mutations occurring in untransfected *msh2*$^{-/-}$ MEFs and *hMTH1*-expressing clone 5

Change(s)	Untransfected *msh2*$^{-/-}$		*hMTH1*-expressing clone 5		Reduction factor[a]
	Occurrence (%)	Mutation rate (10^{-7})	Occurrence (%)	Mutation rate (10^{-7})	
Frameshifts	12 (36.4)	11.3	7 (22.6)	0.41	27.6
Transitions					
G·C → A·T	1 (3.0)	0.9	0		
A·T → G·C	8 (24.2)	7.5	3 (9.7)	0.17	44.1
Transversions					
A·T → C·G	3 (9.1)	2.8	15 (48.4)	0.87	3.2
A·T → T·A	4 (12.1)	3.7	1 (3.2)	0.06	61.7
G·C → C·G	2 (6.1)	1.9	3 (9.7)	0.17	11.2
G·C → T·A	2 (6.1)	1.9	1 (3.2)	0.06	31.7
Large deletions	1 (3.0)	0.9	1 (3.2)	0.06	15.0
Total	33	3.1	31	0.18	17.2

[a] Fold decrease in the mutation rate in *hMTH1*-expressing clone 5.

Western blot analysis indicated that all hMTH1-expressing clones remained *msh2* defective (data not shown).

These findings indicate that a substantial fraction of mutations arising in *msh2*-defective MEFs are prevented by improved dNTP pool sanitation. In particular, a 50-fold-increased hMTH1 expression level effectively abolishes the mutator phenotype associated with *msh2* deficiency. Incorporation of oxidized dNTPs is therefore a major contributor to the mutator phenotype of *msh2*$^{-/-}$ MEFs.

hMTH1 and the *hprt* mutational spectrum. hMTH1 hydrolyzes several oxidized purine dNTPs, including 8-oxodGTP, 2-oxodATP, and 8-oxodATP (20). In order to investigate the contribution of these oxidized precursors to spontaneous mutagenesis in MMR-defective cells, we compared spontaneous *hprt* mutational spectra in *msh2*$^{-/-}$ MEFs and *hMTH1*-overexpressing clone 5. Independent mutants from both cell lines were sequenced. Table 2 shows the frequency and rate of each type of mutation for each cell line. As expected for MMR-deficient cells, frameshifts were the major single mutational type in *msh2*$^{-/-}$ MEFs. They comprised more than one-third of all mutations (12 of 33; 36.4%). Base substitutions comprised around 60% of the total and were equally distributed between transitions and transversions (27.2 and 33.4%, respectively). There was a significant predominance of AT → GC over other transitions (8 of 33 mutations; 24.2%), whereas the four possible transversions were approximately equally represented.

hMTH1 expression in clone 5 cells altered the distribution of mutations. The contributions of frameshifts and transitions were both reduced. When the differences in mutation rate between *msh2*$^{-/-}$ MEFs and clone 5 are taken into account, hMTH1 expression decreased the rates of frameshifts 27.6-fold and of A · T → G · C transitions 44.1-fold. There was a more modest effect on the rate of transversions, which was reduced only 8.9-fold. AT → TA and GC → TA mutations were particularly affected, whereas there was a surprisingly minimal impact on A → C transversion rates, which were reduced only 3.2-fold.

The type and location of the mutation, the surrounding sequence, and the resulting amino acid change are summarized in Table 3 and Fig. 2. Base substitutions appeared to be randomly distributed, although there was some clustering, e.g., the four base substitutions at position 581 in clone 5. In a single case (mutant 53), a double mutation, formed by two TA → GC transversions within three base pairs, was found in clone 5. In contrast, essentially all frameshifts were located within the run of six consecutive guanines at positions 207 to 213, which are a known frameshift hot spot in MMR-defective cells (30). Within this hot spot, all of the mutations scored were −1 deletions. A single +G frameshift was observed in clone 5, and it was located in a nonrepetitive sequence. We conclude that overexpression of hMTH1 reduced the rate of −1 frameshift mutations within the acknowledged G_6 target by 34-fold. Thus, improved dNTP pool sanitation has a profound effect on the incidence of the type of mutations that are regarded as signatures of MMR deficiency. The striking reduction in frameshifts in the G_6 target suggests that incorporation of 8-oxodGMP influences the generation of these mutations in an MMR-deficient cell.

hMTH1 overexpression and the mutator phenotype in MMR-defective human cells. To determine whether improved dNTP pool sanitation affected the mutator phenotype of MMR-defective human cells, hMTH1 was overexpressed in the *hMSH6*-defective human colorectal carcinoma DLD1 cells. Clone 2A expressed a 10-fold-increased level of hMTH1, as determined by enzyme assay and Western blotting. This is comparable to that of clone 2 of the transfected *msh2*$^{-/-}$ MEFs (Fig. 3A). This increased hMTH1 expression reduced steady-state DNA 8-oxoG from 2.6 residues per 10^6 dGMP residues in DLD-1 to 0.9 residues per 10^6 residues in DLD1/clone 2A. The spontaneous *HPRT* mutation rate also decreased by two- to threefold in two independent experiments: from 3.9×10^{-6} to 1.5×10^{-6} per cell/generation and from 2.4×10^{-6} to 1.2×10^{-6} per cell/generation (Fig. 3B). These changes are comparable to those we observed in *msh2*$^{-/-}$ MEFs expressing similar levels of hMTH1. Oxidized purine deoxynucleotides make a significant contribution to the mutator phenotype of these MMR-defective human colorectal carcinoma cells.

MSI is the most dramatic manifestation of the mutator effect in MMR-deficient human tumors. We therefore examined whether hMTH1 expression affected MSI in DLD-1. Single nucleotide frameshifts within mononucleotide repeats predominate in these *hMSH6*-defective cells (6). We therefore examined the *BAT26* mononucleotide repeat (A_{26}) microsatellite. Subclones of DLD-1 and of DLD-1/clone 2A were isolated by single-cell plating, and the *BAT26* repeat was analyzed by PCR. *BAT26* alleles were altered in 16 (44%) of 36 DLD-1 subclones. This corresponds to a mutation rate of 10.8×10^{-3} per generation at this locus. Expression of hMTH1 in DLD-1/clone 2A reduced the frequency of *BAT26* mutation threefold, to 15% (6 of 40; Fisher exact test, $P = 0.003$), corresponding to a rate of 3.6×10^{-3} per generation (Fig. 3C). A similar analysis of the *BAT25* (A_{25}) locus did not reveal a difference between DLD1 and DLD-1/clone 2A, however. The overwhelming majority of changes in *BAT26* were base losses. This bias was also observed in the hMTH1-expressing clones. Thus, hMTH1 expression clearly influences MSI by reducing the frequency of

TABLE 3. Spontaneous mutations in *hprt* locus of untransfected *msh2*$^{-/-}$ MEFs and *hMTH1*-expressing clone 5

Site	Target sequence[a]	Mutation	Codon	Amino acid change	Mutant(s)
msh2$^{-/-}$					
58	CCTAGATTT	G→T	GAT→TAT	Asp→Tyr	9
191	GTGGCCCTC	C→G	GCC→GGC	Ala→Gly	2
202	TGTGCTCAA	C→T	CTC→TTC	Leu→Phe	23
217	CTATAAGTT	A→G	AAG→GAG	Lys→Glu	18, 37
249	TTAAAGCAC	A→G	AAA→AAG	Stop	26
257	CTGAATAGA	A→C	AAT→ACT	Asn→Thr	39
265	AAATAGTGA	A→T	AGT→TGT	Ser→Cys	1
296	GATTTTATC	T→C	TTT→TCT	Phe→Ser	32
305	AGACTGAAG	T→A	CTG→CAG	Leu→Gln	13
309	TGAAGAGCT	G→C	AAG→AAC	Lys→Asn	15
207–213	AAGGGGGGCT	−G			6, 7, 11, 20, 21, 27, 30, 33, 38, 42, 49
385	AAAGAATGT	A→T	AAT→TAT	Asn→Tyr	12
409	TATAATTGA	A→T	ATT→TTT	Ile→Phe	19
476	GTTAAGGTT	A→C	AAG→ACG	Lys→Thr	4, 45
496	GGTGAAAAG	A→G	AAA→GAA	Lys→Glu	35
599	TTCAGGAAT	G→T	AGG→AGT	Arg→Met	29
601–602	CAGGAATTT	−A			25
611	AATCACGTT	A→G	CAC→CGC	His→Arg	28
643	AGCCAAATA	A→G	AAA→GAA	Lys→Glu	36
668	CGCAAGTTG	A→G	AGT→GGT	Ser→Gly	14
668–691		Deletion (−24)			16
Clone 5					
1	GTCATGCCG	A→C	ATG→CTG	Met→Leu	20
143	GAAAGACTT	G→C	AGA→ACA	Arg→Thr	29
197	CTCTGTGTG	G→C	TGT→TCT	Cys→Ser	12
207–213	AAGGGGGGCT	−G			4, 5, 9b, 21, 43
208	CAAGGGGGG	G→T	GGG→TGG	Gly→Trp	18b
227	TTTGCTGAC	C→G	GCT→GGT	Ala→Gly	36
230	GCTGACCTG	A→G	GAC→GGC	Asp→Gly	27a
249	TTAAAGCAC	A→T	AAA→AAT	Lys→Asn	47b
290	ACTGTAGAT	T→G	GTA→GGA	Val→Gly	25
349	AGTTATTGG	A→C	ATT→CTT	Ile→Leu	13
370	CTCAACTTT	A→C	ACT→CCT	Asn→Pro	2
409	ATAATTGAC	A→C	ATT→CTT	Ile→Leu	14, 27
459–485		Deletion (−27)			40
521	GGAT ACA	+G			7
563	GTTGTTGGA	T→G	GTT→GGT	Val→Gly	7a
581	CTTGACTAT	A→G	GAC→GGC	Asp→Gly	26
581	CTTGACTAT	A→C	GAC→GCC	Asp→Ala	28, 54, 23b
601–602	CAGGAATTTG	−A			41
618	GTTTGTGTCAT	T→G	TGT→TGG	Cys→Trp	34
618	GTTTGTGTCAT	T→G	TGT→TGG	Cys→Trp	53*
620	GTTTGTGTCAT	T→G	GTC→GGC	Val→Gly	53*
639	GAAAAGCCA	A→C	AAA→AAC	Lys→Asn	6b
643	AAGCCAAATAC	A→G	AAA→GAA	Lys→Glu	10
647	AAATACAAA	A→C	TAC→TCC	Tyr→Ser	35

[a] Nucleotides affected are in boldface.

−A deletions in *BAT26*. The unchanged mutation rate at *BAT25* suggests that the contribution of oxidized purines is influenced by the sequence context of the repeat.

We also examined the effect of hMTH1 on MSI in the human prostatic cancer cell line DU145. This MMR-defective cell line has a profound mutator phenotype and bears mutations in both the *hMLH1* and *hMSH3* MMR genes (9). The *BAT26* mutation rate was reduced 1.3-fold by 10-fold-increased hMTH1 activity in a clonal isolate (DU145/clone 1). More strikingly, hMTH1 expression dramatically altered the nature of the changes at *BAT26*. All (38 of 38) *BAT26* mutations in DU145 were single A deletions. In contrast, there were only 2 deletions (of 27) among DU145/clone 1 mutations. This indicates that hMTH1 has a selective effect in reducing −1-base changes. This possibility was explored further by analyzing the *SMT15* locus, which contains a run of eight G's. Increased hMTH1 expression in DU145/clone 1 reduced the mutation rate at this locus 10-fold (Fig. 3C). Again, all of the changes in DU145 were −G deletions. Examples of changes at *BAT26* and *SMT15* are shown in Fig. 3D. Thus, *BAT26* and *SMT15* provide clear evidence that oxidized NTPs have a significant influence on MSI. This can affect both A and G repeat microsatellites. The stability of *BAT25* indicates that exceptions do exist and that additional factors, such as surrounding se-

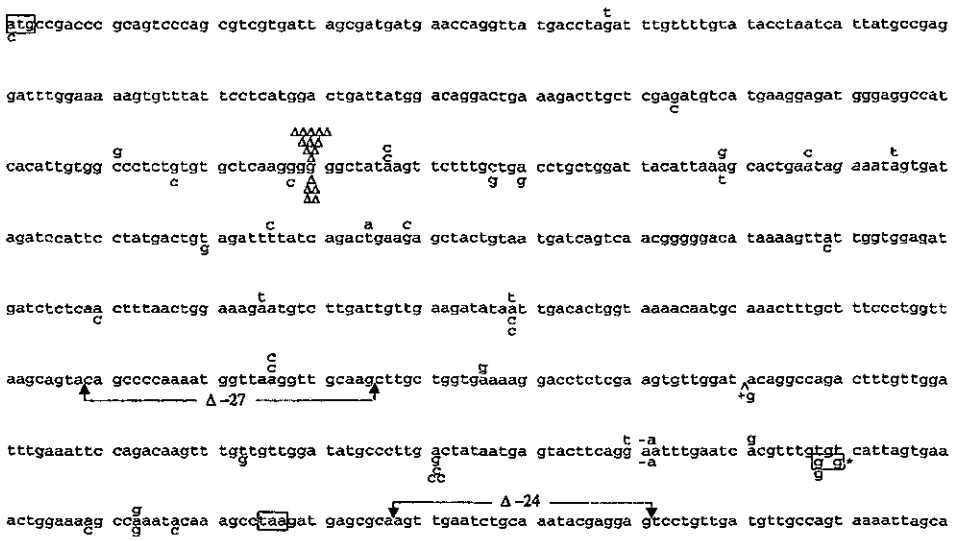

FIG. 2. Locations of *hprt* mutations in *msh2*$^{-/-}$ MEFs and in clone 5. Changes found in *msh2*$^{-/-}$ MEFs and in clone 5 are shown above and below the sequence, respectively. Deletions are indicated by Δ and are single bases unless otherwise indicated. +g is a single-base insertion. The asterisk indicates a double mutant.

quences, may also play a part. The selective effect of hMTH1 expression in reducing the frequency of −1-base deletions is particularly noteworthy.

Thus, hMTH1 expression affects two of the defining characteristic of MMR-defective cells. It reduces *HPRT* mutation rates. It also significantly ameliorates MSI at some, but not all, loci by preventing −1-base deletions. We conclude that the pool of oxidized purine dNTPs significantly influences the mutator phenotype of MMR-defective cells.

DISCUSSION

We previously demonstrated that the oxidized dNTP pool makes a significant contribution to the steady-state level of oxidized purine bases in DNA of MMR-defective cells and suggested that this is likely to be an important factor in their genomic instability (14). Here we provide direct evidence that improved dNTP pool sanitation attenuates two defining features of genetic instability in MMR-defective cells. Overexpression of hMTH1 in *msh2*$^{-/-}$ MEFs reduced mutation rates in the expressed *hprt* gene. It influenced the incidence of several different types of base substitution and prevented frameshifts in the acknowledged G_6 target in this gene. Overexpression of hMTH1 in two MMR-defective human cell lines significantly reduced instability at mononucleotide repeats, indicating that oxidized dNTPs are a significant contributor to MSI. This effect was to some extent locus dependent and selectively affected −1-base changes.

The mutational spectrum in *msh2*$^{-/-}$ MEFs that express a high level of hMTH1 provides important clues to the events underlying their mutator phenotype. The range of hMTH1 substrates includes 8-oxodGTP, 2-oxodATP, and 8-oxodATP (20). One important implication of our data is that incorporation of both oxidized guanine and adenine contributes significantly to the mutator effect of MMR-defective cells. By comparison to 8-oxoadenine (47), 8-oxoG and 2-oxoA are both considered to be highly mutagenic. The pairing properties of 2-oxoA are particularly promiscuous, and it can direct incorporation of dCMP or dAMP to produce AT → GC transitions and AT → TA transversions, respectively (28). The most dramatic effect of hMTH1 expression was on the last two classes of base substitutions. AT → GC and AT → TA mutation rates decreased 44- and 62-fold, respectively. The most straightforward explanation for these findings is that during replication, 2-oxodAMP is incorporated opposite T. In the absence of MMR, the oxidized purine persists and forms the premutagenic mismatches 2-oxoA · C and 2-oxoA · A in the following round of replication (*Fig. 4*). It is interesting that a large increase in mutations at A · T base pairs is the major factor in the increased mutator phenotype of thymic lymphomas that arise in *msh2*$^{-/-}$ mice (50).

2-OxodAMP is also directly mutagenic. It can be incorporated opposite G (27) to generate GC → TA transversions (24, 38). Consistent with a simple reduction in the level of 2-oxodAMP incorporation, hMTH1 expression also prevented this type of mutation. We note, however, an alternative route by which these mutations may arise that is also susceptible to modulation by hMTH1. GC → TA transversions are signature mutations of template 8-oxoG. They could arise at persistent 8-oxodGMP that was incorporated in a previous replication round (Fig. 4). The contribution of persistent 8-oxodGMP is likely to be minimized by BER mediated by Ogg-1 and Myh, both of which are fully operative in these MMR-defective cells. We suggest that reversing the potentially mutagenic incorporation of 2-oxodAMP is a previously unrecognized function of MMR.

The minimal impact of hMTH1 expression (only threefold) on AT → CG transversions is surprising. These mutations arise via the A · 8-oxoG mismatches that are an acknowledged product of 8-oxodGMP incorporation in in vitro replication systems (40). In addition, the mutator phenotype of *E. coli mutT* mutant strains is largely due to increases in this class of

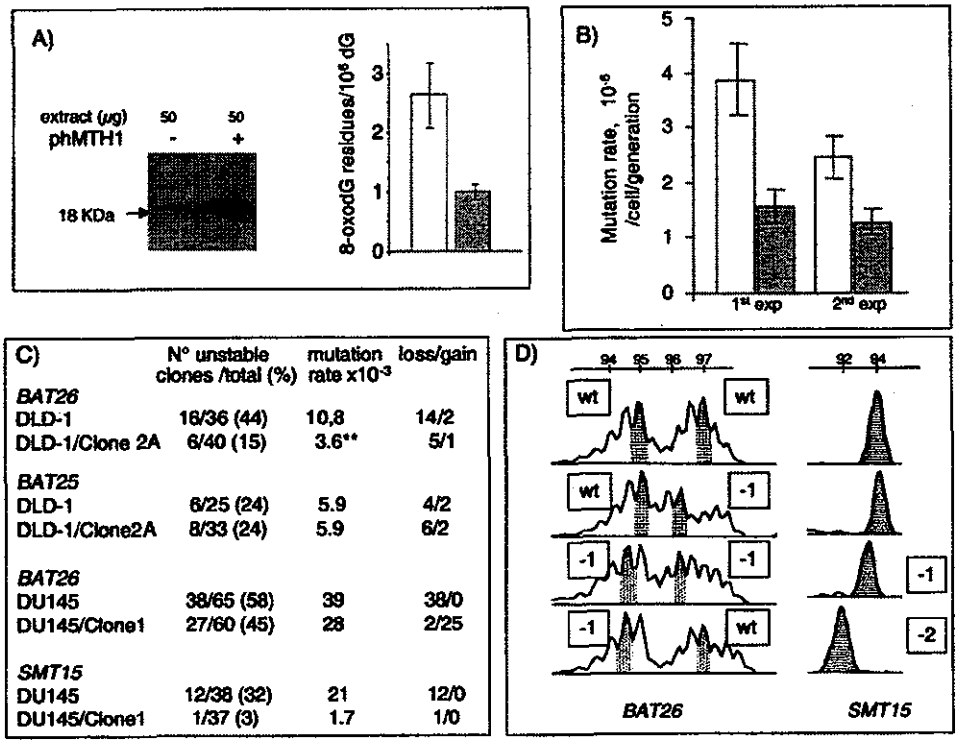

FIG. 3. hMTH1 overexpression and the mutator phenotype of MMR-defective human cells. (A) Western blotting and steady-state levels of DNA 8-oxoG in untransfected DLD-1 (− and unfilled bar) and hMTH1-overexpressing clone 2A (+ and filled bar). Values for 8-oxoG determinations are the mean ± standard deviation of three independent experiments. (B) *HPRT* mutation rates in untransfected DLD-1 (unfilled bars) and clone 2A (filled bars). Two independent determinations are shown. (C) MSI at *BAT26*, *BAT25*, and *SMT15*. DNAs from independent subclones of untransfected DLD-1 and DU145 and their *hMTH1*-overexpressing clones (DLD-1/clone 2A and DU145/clone 1) were amplified by PCR. The total number and the number of unstable clones are shown together with the percentage of unstable clones. Mutation rates were calculated as follows: number of unstable clones/total number of clones × number of generations. The number of clones with −1/−2 changes (loss) or +1/+2 changes (gain) is indicated. (D) Examples of MSI at *BAT26* and *SMT15* in DU145. The values designate different allele sizes. The alterations are shown next to the appropriate panel. wt, wild type.

transversions (2). The modest effect of hMTH1 overexpression suggests that the majority of AT → CG transversions in an MMR-defective background are the consequence of A · G mismatches.

One of the most significant findings is the dramatic reduction in −G frameshifts in the G_6 tract of the *hprt* gene. This identifies oxidized dNTPs as a major contributor to frameshift mutagenesis in these *msh2*$^{-/-}$ cells—a finding that is consistent with the reported phenotype of *mth1* knockout mice. Although these animals do not have an overt mutator phenotype, they do display an increased frequency of −A frameshifts in mononucleotide runs of the transgenic *rpsL* gene (19). We conclude that, in addition to causing base substitutions, oxidized dNTPs make a significant contribution to the production of −1-base frameshifts that are normally corrected by the mouse MMR system.

Increased hMTH1 expression in the two MMR-deficient human cell lines provided further evidence that oxidized dNTPs contribute to the mutator effect of repair-defective cells—and that they particularly influence frameshifts. Although we were unable to isolate transfectants with high hMTH1 expression, a modest level had a significant impact on the phenotype of both DLD-1 and DU145. The *HPRT* mutation rate in DLD-1 was reduced between two and threefold. Since the majority of *HPRT*$^-$ mutations in these *hMSH6*-deficient cells are base substitutions—with a relatively minor contribution from frameshifts (5, 34)—these data are consistent with hMTH1 preventing base substitutions in human *HPRT* as it does in its mouse counterpart. hMTH1 expression in DLD-1 also provided evidence of a significant impact on frameshifts—and by implication on MSI. The mutation rate at *BAT26* was reduced about threefold. Although hMTH1 expression in *hMHL1*-defective DU145 did not produce a measurable decrease in the overall *HPRT* mutation rate (unpublished observation), it confirmed the influence on frameshifts. Although the decrease in the mutation rate at *BAT26* was modest, it was accompanied by a 10-fold reduction in the rate in the G_8 tract of *SMT15*. There were also important qualitative changes. Loss of the hMLH1 (but also of hPMS2 or hMSH2) MMR proteins in human tumor cell lines leads to an accumulation of +G frameshifts in the G_6 target sequence of the *HPRT* gene (5, 39, 22). hMTH1 expression in the human cell lines, as in the *msh2*$^{-/-}$ MEFs, selectively affected minus frameshifts. This was apparent at both *BAT26* and *SMT15*. Thus, oxidized dNTPs contribute to the generation of single-base deletions in repetitive mononucleotide sequences of MMR-defective human and mouse cells.

These findings have two important implications. The first

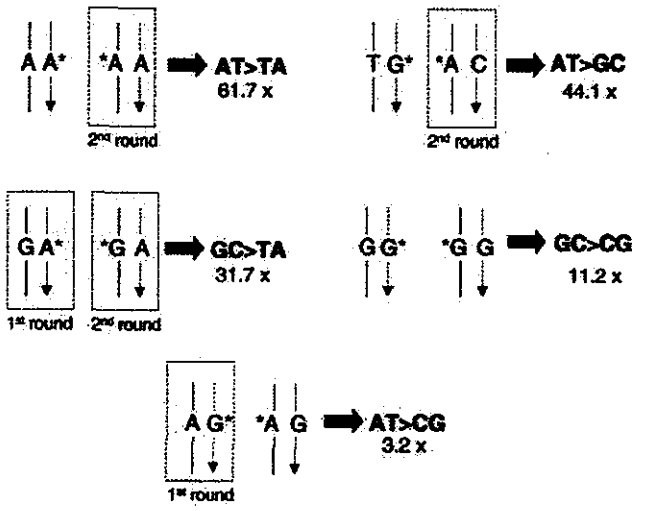

FIG. 4. Oxidized purines and mutations in *msh2*$^{-/-}$ MEFs expressing hMTH1. The major mutational types that are modulated by hMTH1 expression (fold decrease in rate indicated) are shown. It is proposed that mutations arise via oxidized purines that are incorporated into the daughter DNA strand (dotted line, arrowed) during DNA replication. In some cases, the same mutations can be derived from replication of template oxidized base incorporated during a previous round of replication. These are shown where appropriate. Base pairs involving oxidized bases shown boxed are those that have been previously identified by studies using purified DNA polymerases or inferred from in vitro replication studies. Template strands are designated by solid lines. AT → TA transversions and AT → GC transitions are considered to arise from incorporation of 2-oxodAMP opposite the correct base and miscoding of oxidized A (A*) present in the parental strand in the second round of replication (28). Incorporation of 2-oxodAMP opposite a G (24, 38) or miscoding of 8-oxoG when present in the template strand might both lead to GC → TA transversions (46, 12). GC → CG transversions derive from G* · G mismatches. DNA polymerase eta is indeed able to direct, at low efficiency, the incorporation of guanine opposite a template 8-oxoG (23, 48). Incorporation of 8-oxodGMP opposite an A by replicative DNA polymerases (40) is the most plausible mismatch originating AT → CG transversions.

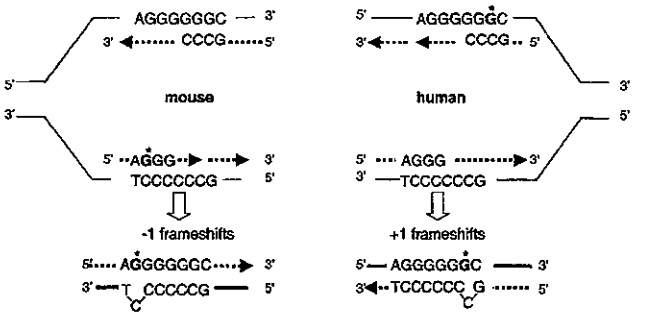

FIG. 5. Model of frameshift formation in the *hprt* gene following 8-oxodGMP incorporation. In human cells, the origin of replication has been mapped in the first intron and the transcribed strand containing G_6 is replicated by the lagging-strand polymerase (13). The location of the origin in mouse cells is unknown. The leading and lagging strands are indicated by arrowed, dotted lines. In mouse cells, −1 frameshifts might arise via an IDL of the C-containing template strand favored by an 8-oxoG in the lagging daughter DNA strand. The inversion in the types of frameshifts in human cells (+G) could be related either to the incorporation of the oxidized purine by a leading-strand DNA polymerase or to the presence of an 8-oxoG in the template strand favoring +1 frameshifts via unstacking of the pyrimidine-containing primer strand during lagging-strand synthesis.

concerns the designation of MSI. There are two A_n mononucleotide runs in the recommended panel of microsatellites (8). Our findings indicate that instability at *BAT26* is likely to be influenced by changes in oxidative metabolism that increase steady-state levels of oxidized purine dNTPs. Secondly, the selective influence of oxidized dNTPs on −1 deletions has implications for the measurement of mutation rates. *HPRT* provides a particularly good example. In MMR-defective mouse cells, most *hprt* mutations are −G frameshifts in a G_6 sequence. The same G_6 sequence is a target in MMR-defective human cells, but in this case, mutations are overwhelmingly +G. Our data indicate that changes in oxidized purine dNTP levels have a more profound influence on −1-base alterations than on +1-base changes. The effect on mutation rates in MMR-defective cells of deranged oxidative metabolism and changes in steady-state oxidized purine dNTPs will therefore depend on the particular genetic target. We note that our data indicate the involvement of oxidized dNTPs in MSI at mononucleotides. Their influence on dinucleotide repeats remains undefined.

The oxidized dNTP that influences frameshifts in BAT26 remains unidentified. The different behaviors of BAT26 and BAT25 are, however, consistent with some of the known properties of 2-oxodATP. 2-OxoA in a double-stranded vector replicated in COS-7 cells induces −A deletions. Importantly, this effect was extremely dependent on both the sequence context of the modified purine and the orientation of its replication. More frameshifts were introduced by lagging-strand 2-oxoA (28). Effects on lagging-strand replication offer a plausible explanation for our finding that oxidized purine dNTPs favor the production of −1-base deletions and may contribute to the qualitative difference between mouse (predominantly −1 changes) and human (predominantly +1 changes) *HPRT* frameshifts (Fig. 5). In human cells, an origin of replication is located in the first intron of *HPRT* (13) and the G_6 sequence is replicated by the lagging-strand DNA polymerase. In the mouse, the origin and direction of replication of the G_6 tract in the third exon are not known. We propose that replication of the G_6 target sequence in mouse cells is in the direction opposite to that of its human counterpart. Minus frameshifts might then arise in the *msh2*$^{-/-}$ mouse cells as a consequence of slippage of the C-containing template strand caused by 8-oxoG in the lagging daughter DNA strand during replication of the C_6 tract. This is consistent with the increased propensity of the lagging-strand DNA polymerase to produce frameshifts compared to the more processive leading-strand polymerases (21, 33). It is also compatible with the acknowledged tendency of mammalian DNA polymerases to produce −1 frameshifts more frequently in runs of template pyrimidines owing to the relatively poor stacking of pyrimidines compared to purines (32). In human cells, the G_6 sequence is replicated by the lagging-strand DNA polymerase and +1 deletions predominate. It is possible that the direction of replication might influence the type of frameshift intermediates generated by oxidized dNTPs.

In summary, the oxidized purine dNTPs—both dATP and dGTP—contribute significantly to the mutator phenotype of MMR-deficient cells. Their effects are quite complex. They

include the simple production of promutagenic mispairings between oxidized purines and normal bases that would usually be subject to correction by MMR. More subtly, they promote the slippage and/or misalignments that are intermediates in frameshift mutation. Their effects on frameshifts are not uniform, and reduction of oxidized dNTP levels is particularly associated with a decreased frequency of −1 deletions in repeated sequences. The extent of the mutator effect will therefore represent a complex interplay among oxidized-dNTP levels, the DNA sequence, and possibly other factors, such as the direction of replication. An important implication of these findings is that the extreme genome instability associated with loss of MMR might be prevented by antioxidant treatment.

ACKNOWLEDGMENTS

This work was supported by grants to M.B. from the Associazione Italiana per la Ricerca sul Cancro, Ministero della Salute and the European Union.

REFERENCES

1. **Aaltonen, L. A., P. Peltomaki, F. S. Leach, P. Sistonen, L. Pylkkanen, J.-P. Mecklin, H. Jarvinen, S. M. Powell, J. Jen, S. R. Hamilton, G. M. Petersen, K. W. Kinzler, B. Vogelstein, and A. de la Chapelle.** 1993. Clues to the pathogenesis of familial colorectal cancer. Science **260**:812–816.
2. **Akiyama, M., T. Horiuchi, and M. Sekiguchi.** 1987. Molecular cloning and nucleotide sequence of the *mutT* mutator of *Escherichia coli* that causes A:T to C:G transversion. Mol. Gen. Genet. **206**:9–16.
3. **Andrew, S. E., M. McKinnon, B. S. Cheng, A. Francis, J. Penney, A. H. Reitmair, T. W. Mak, and F. R. Jirik.** 1998. Tissues of MSH2-deficient mice demonstrate hypermutability on exposure to a DNA methylating agent. Proc. Natl. Acad. Sci. USA **95**:1126–1130.
4. **Andrew, S. E., A. H. Reitmair, J. Fox, L. Hsiao, A. Francis, M. McKinnon, T. W. Mak, and F. R. Jirik.** 1997. Base transitions dominate the mutational spectrum of a transgenic reporter gene in MSH2 deficient mice. Oncogene **15**:123–129.
5. **Bhattacharyya, N., A. Ganesh, G. Phear, B. Richards, A. Skandalis, and M. Meuth.** 1995. Molecular analysis of mutations in mutator colorectal carcinoma cell lines. Hum. Mol. Genet. **4**:2057–2064.
6. **Bhattacharyya, N. P., A. Skandalis, A. Ganesh, J. Groden, and M. Meuth.** 1994. Mutator phenotypes in human colorectal carcinoma cell lines. Proc. Natl. Acad. Sci. USA **91**:6319–6323.
7. **Bianchini, F., S. Elmstahl, C. Martinez-Garcia, A. L. van Kappel, T. Douki, J. Cadet, H. Ohshima, E. Riboli, and R. Kaaks.** 2000. Oxidative DNA damage in human lymphocytes: correlations with plasma levels of alpha-tocopherol and carotenoids. Carcinogenesis **21**:321–324.
8. **Boland, C. R., S. N. Thibodeau, S. R. Hamilton, D. Sidransky, J. R. Eshleman, R. W. Burt, S. J. Meltzer, M. A. Rodriguez-Bigas, R. Fodde, G. N. Ranzani, and S. Srivastava.** 1998. A National Cancer Institute Workshop on Microsatellite Instability for cancer detection and familial predisposition: development of international criteria for the determination of microsatellite instability in colorectal cancer. Cancer Res. **58**:5248–5257.
9. **Boyer, J. C., A. Umar, J. I. Risinger, J. R. Lipford, K. M., S. Yin, C. Barrett, R. D. Kolodner, and T. A. Kunkel.** 1995. Microsatellite instability, mismatch repair deficiency and genetic defects in human cancer cell lines. Cancer Res. **55**:6063–6070.
10. **Branch, P., G. Aquilina, M. Bignami, and P. Karran.** 1993. Defective mismatch binding and a mutator phenotype in cells tolerant to DNA damage. Nature **362**:652–654.
11. **Buermeyer, A. B., S. M. Deschenes, S. M. Baker, and R. M. Liskay.** 1999. Mammalian DNA mismatch repair. Annu. Rev. Genet. **33**:533–564.
12. **Cheng, K. C., D. S. Cahill, H. Kasai, S. Nishimura, and L. A. Loeb.** 1992. 8-Hydroxyguanine, an abundant form of oxidative DNA damage, causes G → T and A → C substitutions. J. Biol. Chem. **267**:166–172.
13. **Cohen, S. M., B. P. Brylawski, M. Cordeiro-Stone, and D. G. Kaufman.** 2002. Mapping of an origin of DNA replication near the transcriptional promoter of the human *HPRT* gene. J. Cell Biochem. **85**:346–356.
14. **Colussi, C., E. Parlanti, P. Degan, G. Aquilina, D. Barnes, P. Macpherson, P. Karran, M. Crescenzi, E. Dogliotti, and M. Bignami.** 2002. The mammalian mismatch repair pathway removes DNA 8-oxodGMP incorporated from the oxidized dNTP pool. Curr. Biol. **12**:912–918.
15. **DeWeese, T. L., J. M. Shipman, N. A. Larrier, N. M. Buckley, L. R. Kidd, J. D. Groopman, R. G. Cutler, H. te Riele, and W. G. Nelson.** 1998. Mouse embryonic stem cells carrying one or two defective *Msh2* alleles respond abnormally to oxidative stress inflicted by low-level radiation. Proc. Natl. Acad. Sci. USA **95**:11915–11920.
16. **Drake, J. W., B. Charlesworth, D. Charlesworth, and J. F. Crow.** 1998. Rates of spontaneous mutation. Genetics **148**:1667–1686.
17. **Duckett, D. R., J. T. Drummond, A. I. Murchie, Y. T. Reardon, A. Sancar, D. M. Lilley, and P. Modrich.** 1996. Human MutSα recognizes damaged DNA base pairs containing O^6-methylguanine, O^4-methylthymine, or the cisplatin d(GpG) adduct. Proc. Natl. Acad. Sci. USA **93**:6443–6447.
18. **Earley, M. C., and G. F. Crouse.** 1998. The role of mismatch repair in the prevention of base pair mutations in *Saccharomyces cerevisiae*. Proc. Natl. Acad. Sci. USA **95**:15487–15491.
19. **Egashira, A., K. Yamauchi, K. Yoshiyama, H. Kawate, M. Katsuki, M. Sekiguchi, K. Sugimachi, H. Maki, and T. Tsuzuki.** 2002. Mutational specificity of mice defective in the *MTH1* and/or the *MSH2* genes. DNA Repair **1**:881–893.
20. **Fujikawa, K., H. Kamiya, H. Yakushiji, Y. Fujii, Y. Nakabeppu, and H. Kasai.** 1999. The oxidized forms of dATP are substrates for the human MutT homologue, the hMTH1 protein. J. Biol. Chem. **274**:18201–18205.
21. **Gawel, D., P. Jonczyk, M. Bialoskorska, R. M. Schaaper, and I. J. Fijalkowska.** 2002. Asymmetry of frameshift mutagenesis during leading- and lagging-strand replication in *Escherichia coli*. Mutat. Res. **501**:129–136.
22. **Glaab, W. E., J. I. Risinger, A. Umar, J. C. Barrett, T. A. Kunkel, J. C. Carrett, and K. R. Tindall.** 1998. Characterization of distinct human endometrial carcinoma cell lines deficient in mismatch repair that originated from a single tumor. J. Biol. Chem. **41**:26662–26669.
23. **Haracska, L., S. L. Yu, R. E. Johnson, L. Prakash, and S. Prakash.** 2000. Efficient and accurate replication in the presence of 7,8-dihydro-8-oxoguanine by DNA polymerase eta. Nat. Genet. **25**:458–461.
24. **Inoue, M., H. Kamiya, K. Fujikawa, Y. Ootsuyama, N. Murata-Kamiya, T. Osaki, K. Yasumoto, and H. Kasai.** 1998. Induction of chromosomal gene mutations in *Escherichia coli* by direct incorporation of oxidatively damaged nucleotides. New evaluation method for mutagenesis by damaged DNA precursors *in vivo*. J. Biol. Chem. **273**:11069–11074.
25. **Jackson, A. L., R. Chen, and L. A. Loeb.** 1998. Induction of microsatellite instability by oxidative DNA damage. Proc. Natl. Acad. Sci. USA **95**:12468–12473.
26. **Jiricny, J.** 2000. Mediating mismatch repair. Nat. Genet. **24**:6–8.
27. **Kamiya, H., and H. Kasai.** 2000. 2-Hydroxy-dATP is incorporated opposite G by Escherichia coli DNA polymerase III resulting in high mutagenicity. Nucleic Acids Res. **28**:1640–1646.
28. **Kamiya, H., and H. Kasai.** 1997. Mutations induced by 2-hydroxyadenine on a shuttle vector during leading and lagging strand syntheses in mammalian cells. Biochemistry **36**:11125–11130.
29. **Kang, D., J. Nishida, A. Iyama, Y. Nakabeppu, M. Furuichi, T. Fujiwara, M. Sekiguchi, and K. Takeshige.** 1995. Intracellular localization of 8-oxo-dGTPase in human cells, with special reference to the role of the enzyme in mitochondria. J. Biol. Chem. **270**:14659–14665.
30. **Kat, A., W. G. Thilly, W.-H. Fang, M. J. Longley, G.-M. Li, and P. Modrich.** 1993. An alkylation-tolerant, mutator human cell line is deficient in strand-specific mismatch repair. Proc. Natl. Acad. Sci. USA **90**:6424–6428.
31. **Kolodner, R. D., and G. T. Marsischky.** 1999. Eukaryotic DNA mismatch repair. Curr. Opin. Genet. Dev. **9**:89–96.
32. **Kunkel, T. A.** 1990. Misalignment-mediated DNA synthesis errors. Biochemistry **29**:8003–8011.
33. **Kunkel, T. A., and K. Bebenek.** 2000. DNA replication fidelity. Annu. Rev. Biochem. **69**:497–529.
34. **Lettieri, T., G. Marra, G. Aquilina, M. Bignami, N. E. Crompton, F. Palombo, and J. Jiricny.** 1999. Effect of *hMSH6* cDNA expression on the phenotype of mismatch repair-deficient colon cancer cell line HCT15. Carcinogenesis **20**:373–382.
35. **Mazurek, A., M. Berardini, and R. Fishel.** 2001. Activation of human MutS homologs by 8-oxo-guanine DNA damage. J. Biol. Chem. **26**:26.
36. **Mo, J.-Y., H. Maki, and M. Sekiguchi.** 1992. Hydrolytic elimination of a mutagenic nucleotide, 8-oxodGTP, by human 18-kilodalton protein: sanitization of nucleotide pool. Proc. Natl. Acad. Sci. USA **89**:11021–11025.
37. **Ni, T. T., G. T. Marsischky, and R. D. Kolodner.** 1999. MSH2 and MSH6 are required for removal of adenine misincorporated opposite 8-oxo-guanine in *S. cerevisiae*. Mol. Cell **4**:439–444.
38. **Nunoshiba, T., T. Watanabe, Y. Nakabeppu, and K. Yamamoto.** 2002. Mutagenic target for hydroxyl radicals generated in *Escherichia coli* mutant deficient in Mn- and Fe-superoxide dismutases and Fur, a repressor for iron-uptake systems. DNA Repair **31**:1–8.
39. **Ohzeki, S., A. Tachibana, K. Tatsumi, and T. Kato.** 1997. Spectra of spontaneous mutations at the *hprt* locus in colorectal carcinoma cell lines defective in mismatch repair. Carcinogenesis **18**:1127–1133.
40. **Pavlov, Y. I., D. T. Minnick, S. Izuta, and T. A. Kunkel.** 1994. DNA replication fidelity with 8-oxodeoxyguanosine triphosphate. Biochemistry **33**:4695–4701.
41. **Shibutani, S., M. Takeshita, and A. P. Grollman.** 1991. Insertion of specific bases during DNA synthesis past the oxidation-damaged base 8-oxodG. Nature **349**:431–434.
42. **Strand, M., T. A. Prolla, R. M. Liskay, and T. D. Petes.** 1993. Destabilization of tracts of simple repetitive DNA in yeast by mutation affecting mismatch repair. Nature **365**:274–276.

43. **Umar, S., A. B. Buermeyer, J. A. Simon, D. C. Thomas, A. B. Clark, R. M. Liskay, and T. A. Kunkel.** 1996. Requirement for PCNA in DNA mismatch repair at a step preceding DNA synthesis. Cell **87**:65–73.
44. **Wei, K., A. B. Clark, E. Wong, M. F. Kane, D. J. Mazur, T. Parris, N. K. Kolas, R. Russell, H. Hou, Jr., B. Kneitz, G. Yang, T. A. Kunkel, R. D. Kolodner, P. E. Cohen, and W. Edelmann.** 2003. Inactivation of exonuclease 1 in mice results in DNA mismatch repair defects, increased cancer susceptibility, and male and female sterility. Genes Dev. **17**:603–614.
45. **Wijnhoven, S. W., H. J. Kool, C. T. van Oostrom, R. B. Beems, L. H. Mullenders, A. A. van Zeeland, G. T. van der Horst, H. Vrieling, and H. van Steeg.** 2000. The relationship between benzo[a]pyrene-induced mutagenesis and carcinogenesis in repair-deficient Cockayne syndrome group B mice. Cancer Res. **60**:5681–5687.
46. **Wood, M. L., M. Dizdaroglu, E. Gajewski, and J. M. Essigmann.** 1990. Mechanistic studies of ionizing radiation and oxidative mutagenesis: genetic effects of a single 8-hydroxyguanine (7-hydro-8-oxoguanine) residue inserted at a unique site in a viral genome. Biochemistry **29**:7024–7032.
47. **Wood, M. L., A. Esteve, M. L. Morningstar, G. M. Kuziemko, and J. M. Essigmann.** 1992. Genetic effects of oxidative DNA damage: comparative mutagenesis of 7,8-dihydro-8-oxoguanine and 7,8-dihydro-8-oxoadenine in Escherichia coli. Nucleic Acids Res. **20**:6023–6032.
48. **Yuan, F., Y. Zhang, D. K. Rajpal, X. Wu, D. Guo, M. Wang, J. S. Taylor, and Z. Wang.** 2000. Specificity of DNA lesion bypass by the yeast DNA polymerase eta. J. Biol. Chem. **275**:8233–8239.
49. **Zhang, L., J. Yu, J. K. Willson, S. D. Markowitz, K. W. Kinzler, and B. Vogelstein.** 2001. Short mononucleotide repeat sequence variability in mismatch repair-deficient cancers. Cancer Res. **61**:3801–3805.
50. **Zhang, S., R. Lloyd, G. Bowden, B. W. Glickman, and J. G. de Boer.** 2002. Thymic lymphomas arising in Msh2 deficient mice display a large increase in mutation frequency and an altered mutational spectrum. Mutat. Res. **500**: 67–74.

Published online June 15, 2004

3198–3211 Nucleic Acids Research, 2004, Vol. 32, No. 10
DOI: 10.1093/nar/gkh642

MUTYH prevents OGG1 or APEX1 from inappropriately processing its substrate or reaction product with its C-terminal domain

Yohei Tominaga, Yasuhiro Ushijima, Daisuke Tsuchimoto, Masaki Mishima[1], Masahiro Shirakawa[2], Seiki Hirano, Kunihiko Sakumi and Yusaku Nakabeppu*

Division of Neurofunctional Genomics, Department of Immunobiology and Neuroscience, Medical Institute of Bioregulation, Kyushu University, Fukuoka 812-8582, Japan, [1]Department of Molecular Biology, Nara Institute of Science and Technology, 8916-5 Takayama, Ikoma Nara 630-0101, Japan and [2]Division of Molecular Biophysics, Science of Biological Supramolecular Systems, Graduate School of Integrated Science, Yokohama City University, Yokohama 230-0045, Japan

Received April 20, 2004; Revised and Accepted May 15, 2004

ABSTRACT

MutY homolog (MUTYH) excises adenine opposite 8-oxoguanine (8-oxoG) in DNA, thus preventing occurrence of G:C to T:A transversion. In cell-free extract prepared from the thymocytes of wild type but not MUTYH-null mice, adenine opposite 8-oxoG in DNA was excised by MUTYH, however, the generated apurinic (AP) site opposite 8-oxoG mostly remained unincised. Recombinant mouse MUTYH (mMUTYH) efficiently excised adenine opposite 8-oxoG and prevented mouse AP endonuclease (mAPEX1) from incising the generated AP site. In contrast, an AP site opposite 8-oxoG created by uracil DNA glycosylase or tetrahydrofuran opposite 8-oxoG was efficiently incised by mAPEX1 in the presence of an excess amount of mMUTYH. Mutant mMUTYH with R361A or G365D substitution, excised adenine opposite 8-oxoG as efficiently as did wild-type mMUTYH, but failed to prevent mAPEX1 from incising the generated AP site. Wild-type mMUTYH bound duplex oligonucleotides containing A:8-oxoG pair with a lower apparent K_d than that of the mutants, and prevented OGG1 from excising 8-oxoG opposite adenine or the generated AP site. The G365D mutant failed to prevent OGG1 from excising 8-oxoG opposite the generated AP site, thus indicating that the protection of its own product by mMUTYH is an intrinsic function which depends on the C-terminal domain of mMUTYH.

INTRODUCTION

Cellular DNA is at high risk of being oxidized by reactive oxygen species, which are inevitably generated by normal metabolic functions such as mitochondrial respiration or by environmental exposure to ionizing radiation and chemicals. The oxidation of DNA appears to result in either spontaneous mutagenesis or cell death and, as a result, it is implicated in various age-related diseases such as cancer and neurodegeneration (1). Among the various types of oxidized damage in DNA, 8-oxoguanine (8-oxoG), an oxidized form of guanine, can pair with adenine as well as cytosine during DNA replication or transcription, and it is thus considered to be one of the spontaneous causes of mutagenesis or cell death (2,3).

Mutator mutants of *Escherichia coli* revealed that the *mutM* (*fpg*) gene encoding 8-oxoG DNA glycosylase which excises 8-oxoG opposite cytosine in DNA, and the *mutY* gene encoding the adenine DNA glycosylase which removes the adenine incorporated opposite 8-oxoG in template DNA, play important roles in the prevention of such spontaneous mutagenesis (4–6). It has been established that most eukaryotic cells also possess either a MutM homolog or its functional homolog, OGG1 for the repair of 8-oxoG, and a MutY homolog (MUTYH or MYH) for the repair of adenine opposite 8-oxoG (7–9).

Prokaryotic MutY and its mammalian homologs MUTYH proteins specifically recognize the adenine base that is misincorporated opposite 8-oxoG present in the template strand, and excise the adenine base by their intrinsic DNA glycosylase activity. The generated AP site opposite 8-oxoG by MUTYH is likely to be processed by the multi-enzyme base excision repair (BER) pathway to yield C:8-oxoG pair, which is then further processed by the BER pathway initiated by MutM or OGG1 to restore the C:G pair (10).

In *E.coli* and fission yeast, the absence of these repair enzymes resulted in significant increases in the spontaneous mutation rate, especially of G:C to T:A transversion mutation (11,12). Recently, familial alterations in the human *MUTYH* gene have been reported to be possible causative mutations for certain types of familial colorectal tumors without a germ-line mutation in the *APC* gene (13,14). We recently generated MUTYH-null mouse embryonic stem (ES) cells. In the

*To whom correspondence should be addressed. Tel: +81 92 642 6800; Fax: +81 92 642 6791; Email: yusaku@bioreg.kyushu-u.ac.jp

The authors wish it to be known that, in their opinion, the first two authors should be regarded as joint First Authors

MUTYH-null cells carrying no adenine DNA glycosylase activity, the spontaneous mutation rate increased 2-fold in comparison to wild-type cells, thus demonstrating that the absence of the MUTYH function in mammalian cells indeed results in a mutator phenotype (15).

In order to suppress G:C to T:A transversion mutation which is initiated by generation of 8-oxoG in template strand, MUTYH has to specifically excise adenine incorporated into the nascent strand only opposite the 8-oxoG, but not adenine in a template strand to which 8-oxoG is misinserted from the nucleotide pools. Therefore, it is proposed that MUTYH recognizes the nascent strand in association with various cellular proteins, such as PCNA or mismatch repair complex (16,17). After an excision of adenine opposite 8-oxoG, cytosine may be inserted opposite 8-oxoG during the repair synthesis, and thereafter OGG1 has to initiate an excision repair of 8-oxoG, thus resulting in a restoration of the G:C pair (18). In order to understand the molecular mechanism regulating how MUTYH accomplishes the appropriate repair processes, an *in vitro* reconstitution of such repair processes is essential.

In the present study, we examined the repair reaction by mMUTYH in cell-free extracts prepared from mouse thymus glands, and found that mMUTYH can excise adenine opposite 8-oxoG or guanine, however, an efficient incision was observed at the apurinic/apyrimidinic (AP) site generated only opposite guanine. Using recombinant mMUTYH and mAPEX1 proteins, we showed that mMUTYH excises adenine opposite 8-oxoG as well as guanine, and prevents mAPEX1 from incising the generated AP site only opposite 8-oxoG. Furthermore, we found that mutant mMUTYH (R361A or G365D) have a much higher dissociation rate than wild type from duplex DNA containing A:8-oxoG pair. As a result, the mutant protein is considered to lose the ability to prevent OGG1 from excising 8-oxoG opposite adenine or the generated AP site, as well as losing the ability to prevent mAPEX1 from incising the generated AP site opposite 8-oxoG.

MATERIALS AND METHODS

Oligonucleotides

Oligonucleotides shown in Table 1, were obtained from Greiner Japan, and the Hokkaido System Science.

Mouse

By means of gene targeting, we previously established *Mutyh* gene knockout mice (15), and heterozygous mice (*Mutyh*$^{+/-}$) backcrossed to C57BL6/J were maintained.

Cell-free extracts from thymocytes

Thymus glands were isolated from four-week old wild-type C57BL/6J and *Mutyh*$^{-/-}$ mice obtained by mating the *Mutyh*$^{+/-}$ mice. Isolated thymus glands (wet weight 1.6 g from 20 mice) were crushed in phosphate-buffered saline (PBS), and liberated thymocytes were collected by centrifugation at 2100 *g* for 10 min at 4°C. Thymocytes were suspended in 1.6 ml of the lysis buffer (20 mM Tris–HCl (pH 8.0), 1 mM EDTA, 0.25 M NaCl, 1 mM dithiothreitol) on ice, and were disrupted by sonication. The cell-free extracts were clarified by centrifugation at 40 000 *g* for 15 min at 4°C, and were stored at −80°C (19).

Table 1. Oligonucleotides used in this study

Oligonucleotide	Sequence[a]
mY5-D207N	GGT AAC CGG TGT GGT Gaa tGG GAA CGT TT
mY5-Q360A	GTC CTC CTG GTG gct AGG CCT GAC TC
mY3-Q360A	GAG TCA GGC CTa gcC ACC AGG AGG AC
mY5-R361A	CTC CTG GTG CAA gct CCT GAC TCA GGT C
mY3-R361A	GAC CTG AGT CAG Gag cTT GCA CCA GGA G
mY5-F373A	ACT GTG GGA Ggc tCC ATC TGT CAC CTT G
mY3-F373A	CAA GGT GAC AGA TGG agc CTC CCA CAG T
−10T7 promoter	CCC GCG AAA TTA ATA CGA CT
+59T7 terminator	ATA GTT CCT CCT TTC AGC AA
*A	FAM-AGC GGC CAT CGA TAC CGT *CAA* CCT CGA GGA ATT CC
*F	FAM-AGC GGC CAT CGA TAC CGT *CFA* CCT CGA GGA ATT CC
*U	FAM-AGC GGC CAT CGA TAC CGT *CUA* CCT CGA GGA ATT CC
*GO	FAM-GGA ATT CCT CGA GGT *GO* GA CGG TAT CGA TGG CCG CT
A	AGC GGC CAT CGA TAC CGT *CAA* CCT CGA GGA ATT CC
F	AGC GGC CAT CGA TAC CGT *CFA* CCT CGA GGA ATT CC
C	AGC GGC CAT CGA TAC CGT *CCA* CCT CGA GGA ATT CC
G	GGA ATT CCT CGA GGT *GGA* CGG TAT CGA TGG CCG CT
T	GGA ATT CCT CGA GGT *TGA* CGG TAT CGA TGG CCG CT
GO	GGA ATT CCT CGA GGT *GO* GA CGG TAT CGA TGG CCG CT
19-P	FAM-AGC GGC CAT CGA TAC CGT C-phosphate
19-OH	FAM-AGC GGC CAT CGA TAC CGT C-OH
15-P	FAM-GGA ATT CCT CGA GGT-phosphate
15-OH	FAM-GGA ATT CCT CGA GGT-OH

FAM, 5′ end was labeled with FAM; GO, 8-oxoG; F, tetrahydrofuran; U, uracil; phosphate, 3′ end was attached with a phosphate group; OH, 3′ end was with a hydroxy group.
[a]A lower-case letter indicates a base substituted for mutagenesis.

Plasmids

For expression of mMUTYH in *E.coli*, wild-type mouse *Mutyh* cDNA was subcloned into pET32a(+) (Novagen), and resulted plasmid was designated as pET32a-mMUTYH which encodes a fusion protein with thioredoxin (Trx-mMUTYH) (15). cDNAs encoding mutant mMUTYH proteins, mMUTYH(D207N), mMUTYH(R361A), mMUTYH(G365D) and mMUTYH(F373A), which were generated by recombinant PCR (20), using oligonucleotides listed in Table 1, were also subcloned into pET32a(+) to obtain pET32a-mMUTYH (D207N), pET32a-mMUTYH(R361A), pET32a-mMUTYH (G365D) and pET32a-mMUTYH(F373A), respectively. mAPEX1 cDNA (21) was subcloned into an *E.coli* expression vector pQE30 (Qiagen) containing a His^6 tag at the N-terminus, and resulted plasmid was designated as pQE30-mAPEX1. For the expression of hOGG1-1a (hOGG1-1a), hOGG1-1a cDNA was subcloned into pET3d (Novagen), and the resulted plasmid was designated as pET3d-hOGG1-1a (22).

Preparation of recombinant mAPEX1 proteins

The expression of His-mAPEX1 was induced by the addition of 1 mM isopropyl β-D-thiogalactoside (Wako Pure

Chemicals) to the cultures of *E.coli* JM109 cells transformed with pQE30-mAPEX1 following incubation at 37°C for 4 h. Cells were suspended in buffer A [154 mM NaCl/5 mM β-mercaptoethanol/50 mM Tris–HCl (pH 7.5)/0.1 mM PMSF/leupeptin (0.5 μg/ml)/pepstatin (0.5 μg/ml)/chymostatin (0.5 μg/ml)], disrupted by sonication and cell lysates were clarified by centrifugation. His-mAPEX1 protein was purified by aid of TALON superflow metal affinity resin (Clontech), according to the manufacturer's instruction. Fractions contained APEX1 were loaded onto PD-10 desalting column (Amersham Biosciences) equilibrated with buffer B [50 mM Tris–HCl (pH 7.5)/50 mM NaCl/1 mM dithiothreitol/ 1 mM EDTA/5 mM $MgCl_2$/ 5% glycerol], and His-mAPEX1 protein was eluted in buffer B, and stored at −80°C.

Preparation of recombinant Trx-mMUTYH proteins

To obtain a soluble recombinant mMUTYH preparation, thioredoxin-fusion protein (Trx-mMUTYH) was prepared as described previously (23). Briefly, cells expressing Trx-mMUTYH were suspended in buffer C [200 mM KCl/5 mM β-mercaptoethanol/20 mM Hepes-KOH (pH 7.8)/0.1 mM PMSF/leupeptin (0.5 μg/ml)/pepstatin (0.5 μg/ml)/chymostatin (0.5 μg/ml)], were disrupted by sonication and cell lysates were clarified by centrifugation. By aid of the TALON superflow metal affinity resin, Trx-mMUTYH was purified, then fractions containing Trx-MUTYH protein were further separated through Superose 12/30 column (Amersham Biosciences) equilibrated with the buffer C containing 500 m M KCl and 10% glycerol, and fractions containing a single band of Trx-MUTYH were stored at −80°C.

Preparation of recombinant hOGG1-1a protein

The expression of hOGG1-1a was induced by adding 1 mM isopropyl β-D-thiogalactoside to the culture of *E.coli* BL21(DE3) cells transformed with pET3d-hOGG1-1a (24), following incubation at 37°C for 2 h. The cells suspended in lysis buffer [50 mM Tris–HCl (pH7.5)/500 mM KCl/20 mM DTT/0.1 mM EDTA], were disrupted by sonication and the cell lysates were clarified by centrifugation. The supernatant was applied onto DEAE–sepharose column (Amersham Biosciences) equilibrated with the lysis buffer, and proteins recovered in the flowthrough fraction was precipitated by ammonium sulfate (40–75% saturation). Protein was dissolved in buffer D [50 mM potassium phosphate (pH7.5)/10% glycerol/10 mM DTT/0.1 mM EDTA], and applied onto Hitrap-heparin column (Amersham Biosciences) equilibrated with buffer D, and was eluted by a linear gradient of KCl (0–1 M). Fractions containing hOGG1-1a was applied onto Mono-S column (Amersham Biosciences) equilibrated with buffer E [50 mM potassium phosphate (pH6.5)/10 mM DTT/0.1 mM EDTA] and bound protein was eluted by a linear gradient of KCl (0–1 M). Fractions containing hOGG1-1a was further applied onto Hiprep-200 (Amersham Biosciences) equilibrated with buffer F [100 mM potassium phosphate (pH7.8)/100 mM KCl/10 mM DTT/0. 1 mM EDTA], and fractions containing a single 40 kDa band were stored at −80°C.

Determination of the protein concentration

The protein concentration was determined using a Bio-Rad protein assay kit (Bio-Rad) and BSA as the standard.

Nicking assay

A fluorescent dye, 6-carboxy fluorescein-aminohexyl amidite (FAM) was attached to the 5′ end of the strand with a target base or damaged base. Duplex oligonucleotide substrates for a nicking assay were prepared as previously described (24), and the labeled strand was shown with an asterisk as *A, *F, *GO, and so on, as summarized in Table 1. Oligonucleotides with *AP:G or *AP:GO were prepared from oligonucleotides with *U:G or *U:GO reacted with *E.coli* uracil DNA glycosylase (Invitrogen), as previously described (22,25). The standard nicking assay was performed, as previously described (22,25). Briefly, 20 nM duplex oligonucleotide substrates were incubated in 12.5 μl of the reaction buffer (10 mM Tris–HCl pH 7.6, 5 μM $ZnCl_2$, 0.5 mM DTT, 0.5 mM EDTA, 1.5% glycerol, 100 μg/ml BSA) with 60 μg of cell-free extract, or 40 nM Trx-mMUTYH and/or mAPEX1 or 100 nM OGG1 at 37°C for a given time, unless otherwise noted. In the presence of mAPEX1, 0.2 mM $MgCl_2$ was carried over from the buffer B in which mAPEX1 was stored. Next, the reactions were heated in the presence of 0.67N NaOH at 95°C for 5 min, and products were extracted with phenol/chloroform, and precipitated with ethanol. Precipitated products were dissolved in 30 μl of 40% formamide containing 3 μg/ml BlueDextran (Sigma) and 10 mM EDTA, then 3 μl of the mixture was fractionated on 8% long Ranger denatured gel (24 cm length) containing 7 M urea at 30 W for 2 h. Specifically nicked 19-base (MUTYH reaction), or 15-base (OGG1 reaction) length oligonucleotide, labeled with FAM was detected using the model 373 automated DNA sequencer and quantified with GeneScan 3.1 software (Perkin Elmer), according to the manufacturer's instructions.

Gel shift assay

FAM-labeled duplex oligonucleotides (20 nM) was incubated in the reaction buffer with 40 nM Trx-MUTYH and/or 200 nM APEX1 at 37°C for 60 min, unless otherwise noted. Next, the reactions products were fractionated on 4% native polyacrylamide gel (12 cm length) in 0.5 × TBE at 4 W for 3 h. Oligonucleotide labeled with FAM was detected using the model 373 automated DNA sequencer and then it was quantified with GeneScan 3.1 software. The results from one of several independent experiments are presented.

RESULTS

Inefficient incision of the AP site generated after the excision of adenine opposite 8-oxoG by mMUTYH in a cell-free extract

Cell-free extracts were prepared from the thymocytes of wild-type and MUTYH-null mice (Figure 1A, lanes 1, 2), and were incubated with duplex oligonucleotides containing adenine opposite 8-oxoG (*A:GO) or adenine opposite guanine (*A:G), in which the asterisk indicates a base in the FAM-labeled strand. Cleavage of *A-containing strand after NaOH treatment, which cleaves the generated AP sites by β/δ-elimination, was examined (Figure 1B). The cleaved fragments (labeled as 19-P and 19-OH) of both duplex oligonucleotides were detected in the reaction products with wild-type extract but not MUTYH-null extract (Figure 1B,

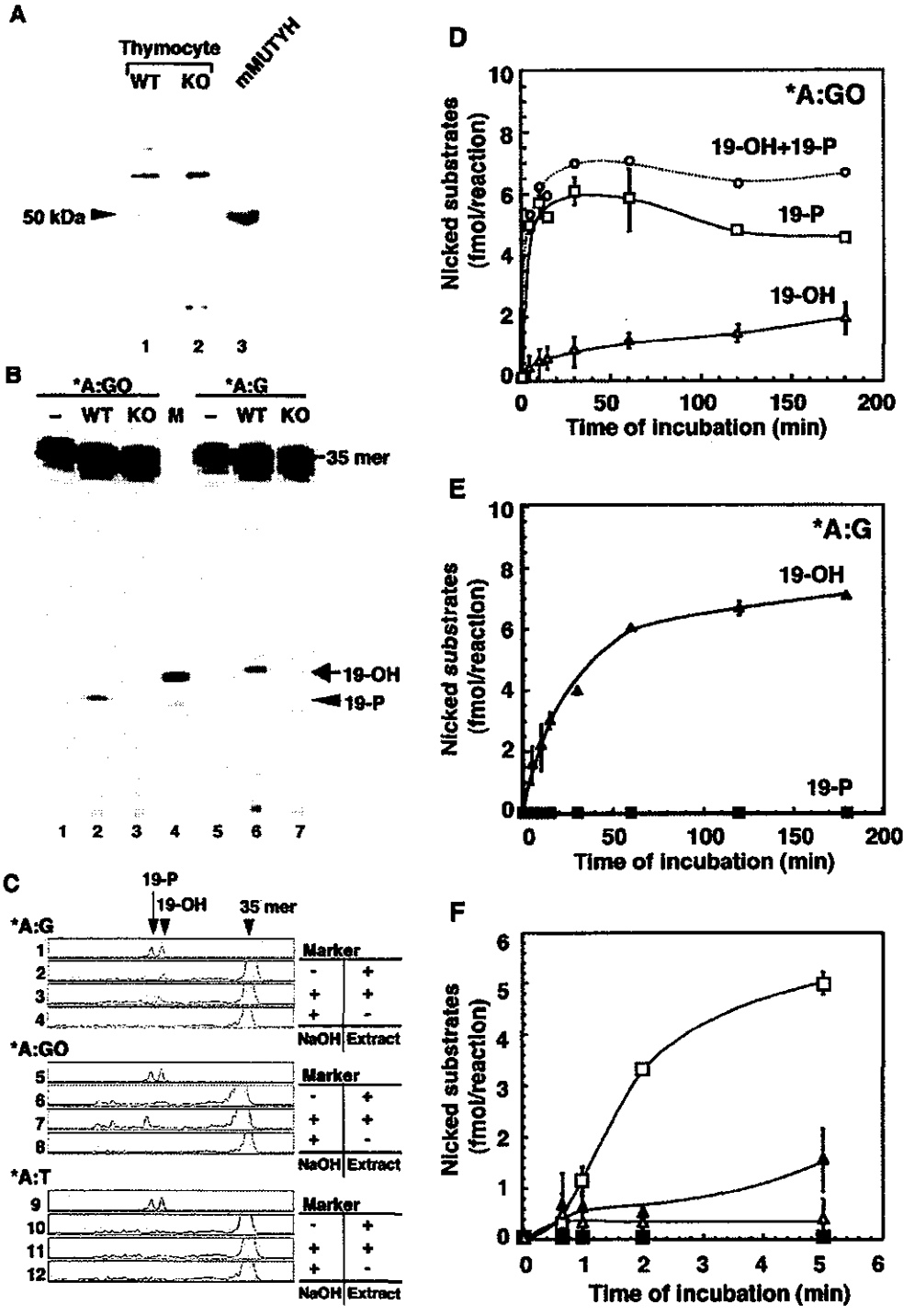

Figure 1. Inefficient incision at an AP site created after excision of adenine opposite 8-oxoguanine by MUTYH in a cell-free extract. (**A**) Thymocyte extracts (30 μg protein per lane) prepared from wild-type (lane 1, WT) and MUTYH-null (lane 2, KO) mice were subjected to western blotting with anti-hMUTYH antibody (25). As a positive control, *in vitro* transcription/translation product (lane 3, mMUTYH) of mouse *Mutyh* cDNA was applied. (**B**) Duplex oligonucleotides (20 nM) containing *A:GO (lanes 1–3) or *A:G (lanes 5–7) were incubated with cell-free extracts (90 μg/12.5 μl reaction) prepared from thymocytes of wild-type (lanes 2, 6, WT) and MUTYH-null (lanes 3, 7, KO) mice for 60 min, and reaction products treated with NaOH were fractionated. Lanes 1, 5, no extract (−); lane 4, marker oligonucleotides (M, 19-OH and 19-P). (**C**) Duplex oligonucleotides containing *A:G (lanes 2–4) *A:GO (lanes 6–8), and *A:T (lanes 10–12) were incubated with (+) or without (−) wild-type cell-free extract as in B, and the reaction mixture treated without (−) or with NaOH (+) was fractionated. The plots obtained by GeneScan are shown. Lanes 1, 5, 9, marker oligonucleotides (19-OH and 19-P). (**D**) Duplex oligonucleotides containing *A:GO were incubated with wild-type cell-free extracts (60 μg/12.5 μl reaction), for the times noted, and reaction products treated with NaOH were fractionated. Open square, production of 19-P; open triangle, production of 19-OH. Open circle, sum of 19-OH and 19-P. (**E**) Duplex oligonucleotides containing *A:G were incubated with wild-type cell-free extracts as in (D). Closed square, production of 19-P; closed triangle, production of 19-OH. (**F**) Preferential action of MUTYH on duplex oligonucleotides containing *A:GO. Results from short-term reactions are shown as in D and E. All data are shown as the means ± S.E.M. of triplicate assays, and the results from one of two independent experiments are presented.

lanes 2, 3, 6, 7), thus indicating that mMUTYH is responsible for the reaction. A fragment co-migrating with a marker oligonucleotide (19-OH) with 3′-OH group corresponds to the incision product by a class II AP endonuclease at the generated AP site after an excision of adenine opposite guanine or 8-oxoG by mMUTYH. Such an incised fragment (19-OH) by AP endonuclease was detected only from duplex oligonucleotides containing *A:G pair but not *A:GO pair (Figure 1B, lanes 2, 6). A fragment co-migrating with a marker oligonucleotide (19-P) with 3′-phosphate, which corresponds to the product cleaved by β/δ-elimination at the generated AP site, was detected in the reaction products from duplex oligonucleotides containing *A:GO pair (Figure 1B, lane 2).

Without NaOH treatment, the 19-OH fragment was also generated from duplex oligonucleotides containing *A:G pair by wild-type extracts (Figure 1C, lane 2), however, neither the 19-P nor the 19-OH fragment was detected in the reaction products from duplex oligonucleotides containing *A:GO pair by wild-type extracts (Figure 1C, lane 6), thus, indicating that wild-type extract excises adenine opposite 8-oxoG but does not incise the generated AP site. No cleaved fragment was detected from the duplex oligonucleotides containing *A:T pair at the corresponding site after incubation with the cell-free extracts, with or without NaOH treatment (Figure 1C, lanes 10, 11).

Addition of 5 mM $MgCl_2$ into the reaction mixture caused non-specific degradation of the substrate (data not shown), probably due to enhanced nuclease activities in the extract. Dialysis of the cell-free extract against the lysis buffer without Mg^{2+}, the activity incising the generated AP site opposite guanine was completely abolished, thus Mg^{2+} or related ions carried over from thymocytes are enough to support the endogenous AP endonuclease activity.

More than two-thirds of the generated AP sites after an excision of adenine opposite 8-oxoG by mMUTYH remained unincised even after 3 h of incubation with the wild-type extract (Figure 1D, open squares), while the rest was slowly incised (Figure 1D, open triangles). In contrast, no unincised AP site was detected in the reaction products from duplex oligonucleotides containing *A:G pair even after a short-term incubation (Figure 1E and F, closed squares). An excision of adenine opposite 8-oxoG by mMUTYH reached a plateau level within 5 min of incubation (Figure 1F, open squares); in contrast, excision of adenine opposite guanine by mMUTYH slowly reached a plateau level after an incubation of >60 min (Figure 1E, closed triangles). These results were also observed in cell-free extracts prepared from splenocytes and ES cells (data not shown).

As a result, mMUTYH more efficiently and rapidly excised adenine opposite 8-oxoG than adenine opposite guanine, thus generating AP sites. The generated AP sites opposite guanine are immediately incised in the cell-free extract, while the AP sites opposite 8-oxoG largely remain unincised, as summarized in Figure 2.

We estimated the content of MUTYH protein in the cell-free extract prepared from wild-type thymocytes to be <10 ng per mg of total protein based on the western blotting findings shown in Figure 1A (lane 1). In the reaction shown in Figure 1D and E, 250 fmol of substrate was incubated with 60 μg of total protein corresponding to 10 fmol or less MUTYH protein, and only 7 fmol of substrates (*A:GO, *A:G) were reacted even after the prolonged incubation, thus indicating that MUTYH exhibits little or no turnover on both substrates with *A:GO and *A:G pairs, as observed for MutY (26).

Recombinant mAPEX1 protein efficiently incises AP sites opposite guanine but not 8-oxoG generated by recombinant mMUTYH protein

To reconstruct the *in vitro* BER reaction initiated by mMUTYH, we prepared recombinant mMUTYH protein fused to thioredoxin (Trx-mMUTYH) and recombinant mAPEX1 with His-tag (His-mAPEX1) (Figure 3A, lanes 1, 5). Purified Trx-mMUTYH possesses an efficient adenine DNA glycosylase activity towards substrates with *A:GO pair with little or no turnover, but not AP lyase activity, since enzymatically incised product was not detected without NaOH treatment at all (Figure 3B, lanes 3–6). These results indicate that Trx-mMUTYH possesses essentially the same catalytic functions as the native MUTYH protein, which also lacks AP lyase activity (22,25).

The incubation of 20 nM substrate with A:GO pair in the presence of 40 nM Trx-mMUTYH resulted in the formation of AP site on ~80% of the substrate, and it is detected as a 19-P fragment after NaOH treatment (Figure 3C, closed circles). In the presence of His-mAPEX1, only a small part of the generated AP site was incised slowly (Figure 3C, open triangles), detected as a 19-OH fragment regardless of NaOH treatment,

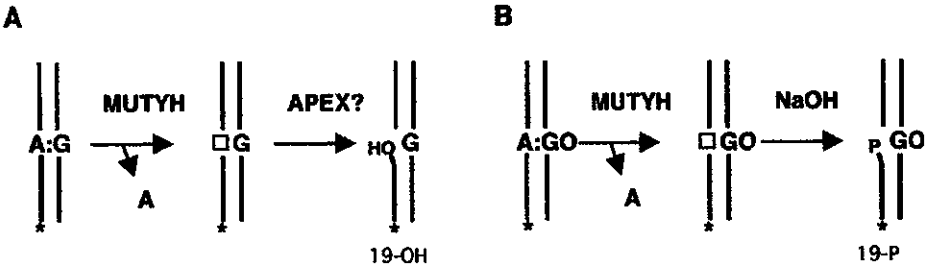

Figure 2. The schematic representation of reaction products generated by MUTYH in the cell-free extracts. mMUTYH excises adenine opposite 8-oxoG or opposite guanine, thus generating an AP site (square). (**A**) The generated AP site opposite guanine is immediately incised by a certain AP enodonuclease (APEX?) in the cell-free extract, and thus the incised fragment with 3′-OH was detected as the 19-OH fragment labeled with FAM(*). (**B**) In contrast, the AP site opposite 8-oxoG remained unincised, and was cleaved by β/δ-elimination catalyzed by NaOH. The cleaved fragment with 3′-phosphate was detected as the 19-P fragment labeled with FAM(*).